

# More Likely Than You Think: Inclination-Driving Secular Resonances are Common in Known Exoplanet Systems

THEA H. FARIDANI <sup>1,2</sup> SMADAR NAOZ <sup>1,2</sup> GONGJIE LI <sup>3</sup> MALENA RICE <sup>4</sup> AND NICHOLAS INZUNZA <sup>1</sup>

<sup>1</sup>*Department of Physics and Astronomy, University of California, Los Angeles, CA 90095, USA*

<sup>2</sup>*Mani L. Bhaumik Institute for Theoretical Physics, Department of Physics and Astronomy, UCLA, Los Angeles, CA 90095, USA*

<sup>3</sup>*School of Physics, Georgia Institute of Technology, Atlanta, GA 30332, USA*

<sup>4</sup>*Department of Astronomy, Yale University, New Haven, CT 06520, USA*

## ABSTRACT

Multi-planet systems face significant challenges to detection. For example, further orbiting planets have reduced signal-to-noise ratio in radial velocity detection methods, and small mutual inclinations between planets can prevent them from all transiting. One mechanism to excite mutual inclination between planets is secular resonance, where the nodal precession frequencies of the planets align such as to greatly increase the efficiency of angular momentum transport between planets. These resonances can significantly misalign planets from one another, hindering detection, and typically can only occur when there are three or more planets in the system. Naively, systems can only be in resonance for particular combinations of planet semimajor axes and masses; however, effects that alter the nodal precession frequencies of the planets, such as the decay of stellar oblateness, can significantly expand the region of parameter space where resonances occur. In this work, we explore known three-planet systems, determine whether they are in (or were in) secular resonance due to evolving stellar oblateness, and demonstrate the implications of resonance on their detectability and stability. We show that about 20% of a sample of three planet transiting systems seem to undergo sweeping resonances early in their lives.

*Keywords:* Exoplanet dynamics (490), Exoplanet evolution (491), Exoplanet formation (492), Planetary system formation (1257)

## 1. INTRODUCTION

The multi-planet Kepler systems, often called “Kepler Multis,” are a class of exoplanet systems uncovered by the *Kepler* mission (Lissauer et al. 2011). They are characterized by hosting 3 or more planets with even spacing (e.g., Weiss et al. 2018), low mutual inclinations (e.g., Lissauer et al. 2011; Fang & Margot 2012; Fabrycky et al. 2014), low eccentricities (e.g., Van Eylen & Albrecht 2015; Van Eylen et al. 2019), and a general absence of mean-motion resonant configurations (e.g., Fabrycky et al. 2014). Moreover, there are suggested correlations in mass and radius of the planets within these systems (i.e., the “Peas in the pod” pattern; Weiss et al. 2018; Millholland et al. 2017). While detection bias may

be a contributing factor in the detection of this pattern (e.g., Murchikova & Tremaine 2020; Zhu 2020), these biases alone cannot realistically account for all the correlations observed (e.g., Weiss & Petigura 2020; Weiss et al. 2023). As these are high-multiplicity exoplanet systems, they experience planet-planet interactions. These interactions have been studied extensively in the literature, and can sculpt the present-day configurations of exoplanet systems both through short-timescale effects like scattering and long-timescale effects like secular evolution (see e.g., Lithwick & Wu 2011; Van Laerhoven & Greenberg 2012; Naoz et al. 2013a; Lanza & Shkolnik 2014; Petrovich et al. 2019; Denham et al. 2019; Volk & Malhotra 2020; Wei et al. 2021; Lu et al. 2024).

As an example of the significance of planet-planet interactions, secular resonances can significantly impact exoplanet systems. Secular resonances can lead to increased rates of angular momentum exchange when certain precessional frequencies align, discussed in detail in

section 2. These frequencies are much slower than the orbital frequency, hence, “secular”. Secular resonances can interact with tides to circularize or migrate planetary orbits (e.g., Hansen & Murray 2015). In systems with three or more planets, resonances can overlap, causing chaotic evolution of planets’ orbits, known as “secular chaos,” which can destabilize systems, produce ultra short-period planets, and pollute white dwarfs (e.g., Lithwick & Wu 2011; Petrovich et al. 2019; O’Connor et al. 2022).

The secular planet-planet interactions can be quantified to linear order in eccentricity and inclination by the well-studied “Laplace-Lagrange” formalism (see, e.g., Ch. 7 of Murray & Dermott 2000). The Laplace-Lagrange formalism models planets and other bodies orbiting a central body (usually a star) as massive rings, which torque and deform each other, changing their eccentricities and inclinations but conserving energy (semimajor axes). Laplace-Lagrange correctly predicts the initial conditions that produce first-order secular resonances (which depend only on the bodies’ masses and semimajor axes). Laplace-Lagrange itself cannot predict higher-order secular resonances, such as those that create “secular chaos” (see, e.g., Lithwick & Wu 2011) that may only appear for particularly excited eccentricity or inclination values. Beyond planet-planet interaction, in recent years, there has been a growing interest in the star-planet interaction, including interactions arising from general relativity, the evaporating protoplanetary disk, and the stellar gravitational quadrupole moment,  $J_2$  (e.g., Plavchan et al. 2015; Faridani et al. 2022, 2023; Spalding & Batygin 2016; Becker et al. 2020; Brefka & Becker 2021; Wei et al. 2021; Chen et al. 2022).

The evolving disk is of particular note because of its time-evolution. Its evolution creates a precession in the planets’ longitudes of ascending node and arguments of periapsis, which can bring them into and out of secular resonance. The time-variation of the precession means that the resonance moves across a (potentially quite large) region of the parameter space rather than staying in place. This is commonly called a “sweeping secular resonance”. If a system is in a region of parameter space where the sweeping resonance occurs, the resonance can imprint a signature on the orbital elements of the planets post-evaporation. Sweeping resonances have been identified in the evolving disk and have been shown to affect planet formation (e.g., Best et al. 2024) and excite significant eccentricity and inclination in nearby planets post-formation (e.g., Heppenheimer 1980; Ward 1981; Nagasawa et al. 2003; Li & Lai 2023; Zanazzi & Chiang 2024; Petrovich et al. 2020).

The stellar gravitational quadrupole moment,  $J_2$  is a correction to the stellar gravitational potential arising from a star’s deviations from spherical symmetry (e.g., Murray & Dermott 2000). This asymmetry causes nodal recession and periapsis precession for any planets orbiting that star at a rate of

$$\dot{\Omega}_{J_2}, \dot{\omega}_{J_2} = \mp n \left[ \frac{3}{2} J_2 \left( \frac{R_\star}{a} \right)^2 \right] \propto \mp J_2 P^{-7/3}, \quad (1)$$

where  $P$  is an individual planet’s orbital period (e.g., Murray & Dermott 2000). The quadrupole moment  $J_2$  was shown to misalign tightly packed planets from one another (e.g., Spalding & Batygin 2016; Becker et al. 2020; Brefka & Becker 2021), impact transit probabilities in single-planet systems (e.g., Stephan & Gaudi 2023) contribute to tidal migration (e.g., Pu & Lai 2019; Millholland & Spalding 2020), and has been used to analyze the orbital inclination of Mercury (e.g., Ward et al. 1976).

For sun-like, main-sequence stars, the evolution of their spins results in a significant evolution of their  $J_2$  values. During their pre-main-sequence phases, sun-like stars have an observed range of spins, from 10-day periods to as fast as one day (e.g., Gallet & Bouvier 2013). However, it is well-known that main sequence stars lose angular momentum via magnetic braking on their stellar wind (e.g., Parker 1958; Schatzman 1962; Kraft 1967; Weber & Davis 1967; Mestel 1968; Skumanich 1972). This spindown can be approximated by a power law for sun-like stars (e.g., Dobbs-Dixon et al. 2004), where faster-spinning stars lose more angular momentum per unit time. Over the first gigayear, this dramatically reduces the dispersion in rotational velocities of sun-like stars, and thereafter their spins evolve slower, following the Skumanich relation of  $\dot{S} \propto t^{-1/2}$  (Skumanich 1972), where  $S$  denotes the stellar spin. More massive stars spin down differently: above the “Kraft Break” at  $T_{\text{eff}} > 6250$  K (Kraft 1967), stars typically experience little angular momentum loss via magnetic braking due to thin convective zones that cannot drive sufficient wind to achieve angular momentum loss.

Most old, sun-like stars have similar spin rates (about a few weeks; Delorme et al. 2011; Meibom et al. 2015; Hartman et al. 2010). The spin of old ( $\sim$ few Gyrs) stars is not correlated with the young stellar spins, and decreases with time (e.g., Barnes 2003; Skumanich 1972). This range of initial conditions and evolution implies that planets are exposed to a wide range of stellar  $J_2$  values during their first gigayear. Therefore, the planets are exposed to a time-varying precession again after the disk evaporates. This can produce a sweeping secular resonance similar to those caused by the evolu-

ing disk. This  $J_2$  sweeping resonance can affect three (or more) planet systems, freezing in excited inclinations and eccentricities [Brefka & Becker \(2021\)](#); [Faridani et al. \(2023\)](#), and can even excite two-planet systems if the inner planet has sufficient angular momentum (e.g., [Spalding & Batygin 2016](#)).

In this work, we focus on observed systems and analyze their secular, planet-planet, and planet-star interaction, with a focus on exploring the potential impact of evolving  $J_2$  on their configuration, and whether evolving  $J_2$  produces sweeping secular resonances in them. We find that about a fifth of all 3-planet observed transiting systems have configurations that indicate they have undergone sweeping resonances due to evolving  $J_2$  in their pasts. This potentially can be used, for example, to constrain the initial conditions of exoplanet systems or to even constrain the initial spin of the host star.

We pedagogically describe the sweeping resonances via the evolving  $J_2$  phenomenon and demonstrate its applicability to observed transiting systems. This paper is structured as follows: in Section 2 we construct the secular model used to explore the secular resonances of interest, in Section 3 we demonstrate the impact of system initial conditions on whether sweeping resonances occur and their strengths, and in Section 4 we apply these calculations to 31 three-planet transiting systems and show approximately one fifth of them may have experienced sweeping resonances in their past. In Section 5 we discuss the implications of these findings and what effects might influence the fraction of systems that encounter inclination-driving secular resonances via evolving  $J_2$ , and in Section 6 we conclude.

## 2. SECULAR RESONANCES AND THE RELATION TO $J_2$

Consider a star with a mass  $M_*$  and a radius  $R_*$ , orbited by a three-planet ( $j = 0, 1, 2$ ) system in which the  $j$ th planet has a mass  $m_j$ , semi-major axis  $a_j$ , period  $P_j$  (orbital frequency  $n_j = 2\pi/P_j$ ), eccentricity  $e_j$ , longitude of ascending node  $\Omega_j$ , longitude of periapsis  $\varpi_j$ , and inclination with respect to the star's spin axis  $I_j$ . A schematic of the system is depicted in Figure 1. For completeness, here, we specify the Laplace-Lagrange equations. Given the secular disturbing function  $\mathcal{R}^{(\text{sec})}$  (e.g., [Murray & Dermott 2000](#))

$$\begin{aligned} \mathcal{R}_j^{(\text{sec})} = & n_j a_j^2 \left[ \frac{1}{2} A_{jj} e_j^2 + \frac{1}{2} B_{jj} I_j^2 \right. \\ & + \sum_{k=1, k \neq j}^N A_{jk} e_j e_k \cos(\varpi_j - \varpi_k) \\ & \left. + \sum_{k=1, k \neq j}^N B_{jk} I_j I_k \cos(\Omega_j - \Omega_k) \right], \end{aligned} \quad (2)$$

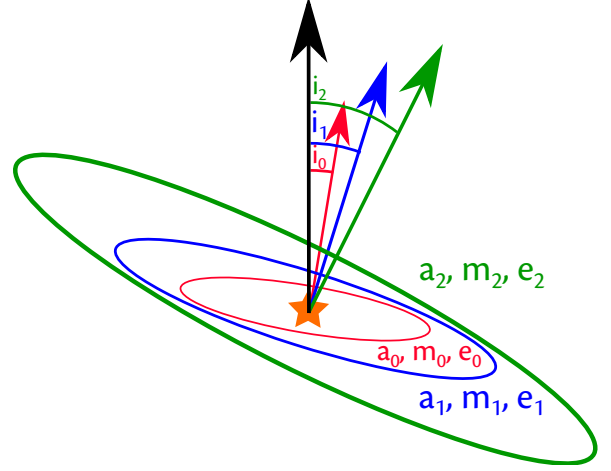


**Figure 1.** A simplified depiction of the three-planet systems considered in this work (not to scale), showing the labeling convention of the planets adopted.

where

$$\begin{aligned} A_{jj} = & n_j \left[ \frac{3}{2} J_2 \left( \frac{R_*}{a_j} \right)^2 \right. \\ & \left. + \sum_{k=1, k \neq j} \frac{m_k}{4\pi (M_* + m_j)} \alpha_{jk} \bar{\alpha}_{jk} f_\psi(\alpha_{jk}) \right], \end{aligned} \quad (3)$$

where  $J_2$  is the quadrupole moment of the star. Additionally,

$$A_{jk} = -\frac{n_j m_k}{4\pi (M_* + m_j)} \alpha_{jk} \bar{\alpha}_{jk} f_{2\psi}(\alpha_{jk}), \quad (4)$$

$$\begin{aligned} B_{jj} = & -n_j \left[ \frac{3}{2} J_2 \left( \frac{R_*}{a_j} \right)^2 \right. \\ & \left. + \sum_{k=1, k \neq j} \frac{m_k}{4\pi (M_* + m_j)} \alpha_{jk} \bar{\alpha}_{jk} f_\psi(\alpha_{jk}) \right], \end{aligned} \quad (5)$$

$$B_{jk} = \frac{n_j m_k}{4\pi (M_* + m_j)} \alpha_{jk} \bar{\alpha}_{jk} f_\psi(\alpha_{jk}), \quad (6)$$

where

$$\alpha_{jk} = \min \left( \frac{a_j}{a_k}, \frac{a_k}{a_j} \right), \quad (7)$$

$$\bar{\alpha}_{jk} = \min \left( \frac{a_j}{a_k}, 1 \right), \quad (8)$$

$$f_\psi(\alpha_{jk}) = \int_0^{2\pi} \frac{\cos \psi}{\left( 1 - 2\alpha_{jk} \cos \psi + \alpha_{jk}^2 \right)^2} d\psi, \quad (9)$$

and

$$f_{2\psi}(\alpha_{jk}) = \int_0^{2\pi} \frac{\cos 2\psi}{\left( 1 - 2\alpha_{jk} \cos \psi + \alpha_{jk}^2 \right)^{\frac{3}{2}}} d\psi. \quad (10)$$

Using the disturbing function, Eq. 2, we can find the time evolution of the system’s orbital parameters as follows

$$\begin{aligned} \dot{e}_j &= -\frac{1}{n_j a_j^2 e_j} \frac{\partial \mathcal{R}_j^{(\text{sec})}}{\partial \varpi_j}, & \dot{\varpi}_j &= +\frac{1}{n_j a_j^2 e_j} \frac{\partial \mathcal{R}_j^{(\text{sec})}}{\partial e_j}, \\ \dot{I}_j &= -\frac{1}{n_j a_j^2 I_j} \frac{\partial \mathcal{R}_j^{(\text{sec})}}{\partial \Omega_j}, & \dot{\Omega}_j &= +\frac{1}{n_j a_j^2 I_j} \frac{\partial \mathcal{R}_j^{(\text{sec})}}{\partial I_j}, \end{aligned} \quad (11)$$

For all planets, a small correction to their  $\varpi$  precessional frequency can be made to account for (to first-order) general relativity,

$$\dot{\omega}_{j,GR} = \frac{3(GM_\star)^{3/2}}{c^2 a_j^{5/2} (1 - e_j^2)}. \quad (12)$$

We include this term for all simulations in this work. However, for all the systems of interest, the planets orbit too far out for this term to ever dominate over the planet-planet interactions or the precession caused by  $J_2$ . In other words, we see that the GR precession term has very little impact in the simulations. Therefore, for our analytic calculations, we omit this term, as it is negligible. Moreover, as GR precession primarily impacts eccentricity evolution (as eccentricity affects the conjugate momentum associated with the  $\varpi$  angle), and in this work we are primarily concerned with inclination evolution, the omission of GR is not expected to have significant impact. When eccentricity evolution is of primary concern, GR can have significant impacts (see e.g., Naoz et al. 2013b; Pu & Wu 2015; Denham et al. 2019; Wei et al. 2021; Faridani et al. 2022; Hansen & Naoz 2020), and can be incorporated into the Laplace-Lagrange  $A$  matrix if desired (see e.g., Marzari & Naga-sawa 2020).

Here, we allow the stellar quadrupole moment to evolve as a function of time, adopting the following relation (e.g., Spalding & Batygin 2016):

$$J_2 = \frac{1}{3} k_2 \left( \frac{S}{S_b} \right)^2, \quad (13)$$

where  $k_2$  is the Love number of the star,  $S$  represents the star’s spin, and  $S_b$  is the breakup spin denoted by  $S_b = \sqrt{GM_\star/R_\star^3}$ . During the main sequence stage, the stellar spin slows down as it loses angular momentum due to magnetic stellar winds – a process known as magnetic braking (e.g., Parker 1958; Schatzman 1962; Weber & Davis 1967; Mestel 1968). We adopt the spindown rate following Dobbs-Dixon et al. (2004),

$$\dot{S} = -\alpha S^3, \quad (14)$$

with  $\alpha = 1.5 \times 10^{-14}$ . The effect on  $J_2$  is shown in Faridani et al. (2023, Figure 1), duplicated here in Figure 2.

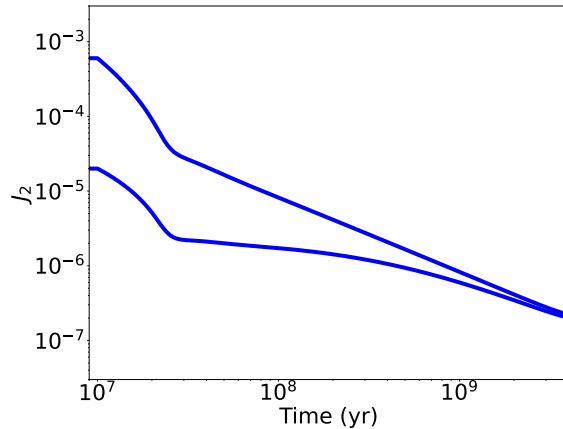


**Figure 2.** Depiction of a range of possible  $J_2$  evolutions for sun-like stars. Figure used with permission from Faridani et al. (2023), and that work describes the models used to generate it.

Briefly, the ranges shown in Figure 2 correspond to the possible range of initial spins for young sun-like stars, and the evolution is derived from Equation 14 and from internal parameters derived from a MESA model (Paxton et al. 2011, 2013, 2015, 2018, 2019; Jermyn et al. 2023). The power-law spin-down relation is chosen for simplicity. The exact functional form of  $J_2$  evolution has little effect as long as  $\dot{J}_2$  is slower than other relevant timescales in the system (see e.g., Becker et al. 2020; Faridani et al. 2023).

In Faridani et al. (2023), we noted that as  $J_2$  evolves, an exoplanetary system may be swept into a resonance that leaves an imprint on the planet’s eccentricity and inclination. In preparation to map the resonances for a wide range of the planets’ parameter space, we first depict an example. Specifically, consider the system Kepler-9 with parameters given in Table 1. The inner planet mass was determined using the mass-radius relation described in Müller et al. (2023).

In Figure 3, we show the time evolution of Kepler-9’s planetary system. Specifically, we show the mutual inclination between the planets (left top panel) and eccentricity (left bottom panel) as well as the alignment or misalignment of the outer two planets’ longitude of ascending nodes (top right panel) and longitudes of periapsis (bottom right panel). Mutual inclinations were obtained by combining  $I_j$  and  $\Omega_j$  to get the 3D planetary angular momentum vector for each planet and the mutual inclination was calculated using a dot product. The initial mutual inclination between the outer planets is chosen to be  $2.5^\circ$ . For simplicity, we adopt that the initial longitudes of ascending node of the planets are set

to (approximately) zero. This evolution was obtained by integrating Equations 11 (which include  $J_2$  precession) and adding GR precession. As Equations 11 are secularly averaged, the evolution in Figure 3 is therefore purely secular.

Initially,  $J_2$  is high, and the eccentricities and mutual inclinations oscillate about their initial value and do not evolve significantly for the first few Myr. This is because the  $J_2$  evolution in Figure 2 remains constant for the first 10 Myr<sup>1</sup>. Then, Kepler-9 is swept into a resonance, exciting Kepler-9d’s eccentricity and inclination, and the outer two planets’ longitudes of ascending nodes lock together ( $\Omega_b = \Omega_c$ ). A similar effect occurs in the eccentricities and longitudes of pericenter ( $\varpi_b = \varpi_c$ ), though at a later time in the evolution. The inclination excitation occurs at  $t \approx 17$  Myr and the eccentricity excitation at  $\approx 22$  Myr.

Clearly, the effects of resonances mediated by  $J_2$  can be drastic. Thus, exploring the maximum inclination (and eccentricity) achieved for a range of  $J_2$  values is a promising avenue for evaluating the impact of evolving  $J_2$  in different systems. For a fixed value of  $J_2$  and neglecting General Relativity precession, the maximum value of the planets’ inclinations over all time can be calculated as follows<sup>2</sup>. Let  $g_i$  and  $f_i$  be the eigenvalues of the matrices  $A$  and  $B$  and  $\bar{e}_{ij}$  and  $\bar{I}_{ij}$  the matrix of normalized eigenvectors of  $A$  and  $B$ . It can be shown that for  $h_j$ ,  $k_j$ ,  $p_j$ , and  $q_j$  defined as

$$\begin{aligned} h_j &= e_j \sin \varpi_j, & k_j &= e_j \cos \varpi_j, \\ p_j &= I_j \sin \Omega_j, & q_j &= I_j \cos \Omega_j, \end{aligned} \quad (15)$$

their time evolution, for a fixed value of  $J_2$ , is

$$\begin{aligned} h_j &= \sum_{i=1}^N e_{ji} \sin(g_i t + \beta_i), & k_j &= \sum_{i=1}^N e_{ji} \cos(g_i t + \beta_i), \\ p_j &= \sum_{i=1}^N I_{ji} \sin(f_i t + \gamma_i), & q_j &= \sum_{i=1}^N I_{ji} \cos(f_i t + \gamma_i), \end{aligned} \quad (16)$$

for scaled  $e_{ji}$  and  $I_{ji}$  defined as,  $S_i \bar{e}_{ji} = e_{ji}$  and  $T_i \bar{I}_{ji} = I_{ji}$ , and phases  $\beta_i$  and  $\gamma_i$ . This time evolution is only true for a fixed value of  $J_2$  because changing  $J_2$  changes the eigenvalues  $g_i$  and  $f_i$ , as  $A_{jj}$  and  $B_{jj}$  are functions of  $J_2$ .

Therefore, for a fixed  $J_2$ , the maximum eccentricity and inclination of planet  $j$  can be calculated by finding the values when all the oscillations are in phase:  $e_{j,\max} =$

$\sum_{i=1}^N |e_{ji}|$ , and  $I_{j,\max} = \sum_{i=1}^N |I_{ji}|$ . To find,  $e_{ji}$  and  $I_{ji}$  the values of the scaling constants  $S_i$ ,  $T_i$  are required.  $S_i$ ,  $T_i$  and the phases  $\beta_i$  and  $\gamma_i$  can be found by solving the linear equations,

$$\begin{aligned} e_{ji} S_i \sin \beta_i &= h_j(t=0), & e_{ji} S_i \cos \beta_i &= k_j(t=0), \\ I_{ji} T_i \sin \gamma_i &= p_j(t=0), & I_{ji} T_i \cos \gamma_i &= q_j(t=0). \end{aligned} \quad (17)$$

These calculations enable analytical prediction of the inclination induced by  $J_2$  if they are repeated for a wide variety of  $J_2$  values.

### 3. THE EFFECT OF INITIAL CONDITIONS ON SECULAR RESONANCES

In Figure 4, we show, for a synthetic three-planet system, the relationship between the semimajor axis ratios between the planets and the subsequent inclination induced on the innermost planet by interactions with the outer planets. Planet radii for the inner, middle, and outer planets, were selected as median radii in that orbital position across the 31 three-planet systems studied in Section 4. Planet masses were calculated using the Mass-Radius relation of Müller et al. (2023). The analytic calculations described in the previous section describe how to calculate the maximum inclination of the inner planet due to planet-planet interactions and  $J_2$  precession for a fixed value of  $J_2$ . To produce the right panel of Figure 4, these calculations were repeated for many  $J_2$  values between  $10^{-3}$  and  $10^{-8}$ , and the maximum inner planet inclination across all  $J_2$  values is shown for each semimajor axis ratio in the grid. This calculation produces five visually distinct regions, which we show heuristically in the left panel. The region boundaries in the left panel were drawn by hand. The notations on the left panel describe how these regions change when parameters are adjusted.

In the leftmost region,  $a_2 \gg a_1$ , there is no resonance, and inclinations induced on the inner planet are small. To the right of this region is a thin strip where inner planet inclination is maximized. This occurs for only a narrow subset of choices of  $a_1$  and  $a_2$ . This region is caused by secular resonances when  $J_2 = 0$  or when  $J_2$  is sufficiently small to be negligible. To the right of the  $J_2 = 0$  resonant region is a much larger region of enhanced inclination. This is caused by secular resonances for a range of nonzero, nontrivial  $J_2$  values. This region is not in resonance for  $J_2 = 0$ , but for every point in the region, there exists some  $J_2 \neq 0$  which precesses the planets just enough to bring the planets into secular resonance. We call this the ‘‘Sweeping Resonance’’ region because for a particular value of  $J_2$ , only a small portion of the region is in resonance, and it is only as  $J_2$  continuously evolves that that resonant portion ‘‘sweeps’’

<sup>1</sup> see Appendix B for a discussion

<sup>2</sup> Including GR does not change the calculation when finding maximum inclinations because GR precesses the argument of pericenter instead of the longitude of ascending node. The maximum eccentricity, however, is affected by GR, and when a planet orbits close enough to its host that it has a period shorter than a few days, this calculation may not be accurate.

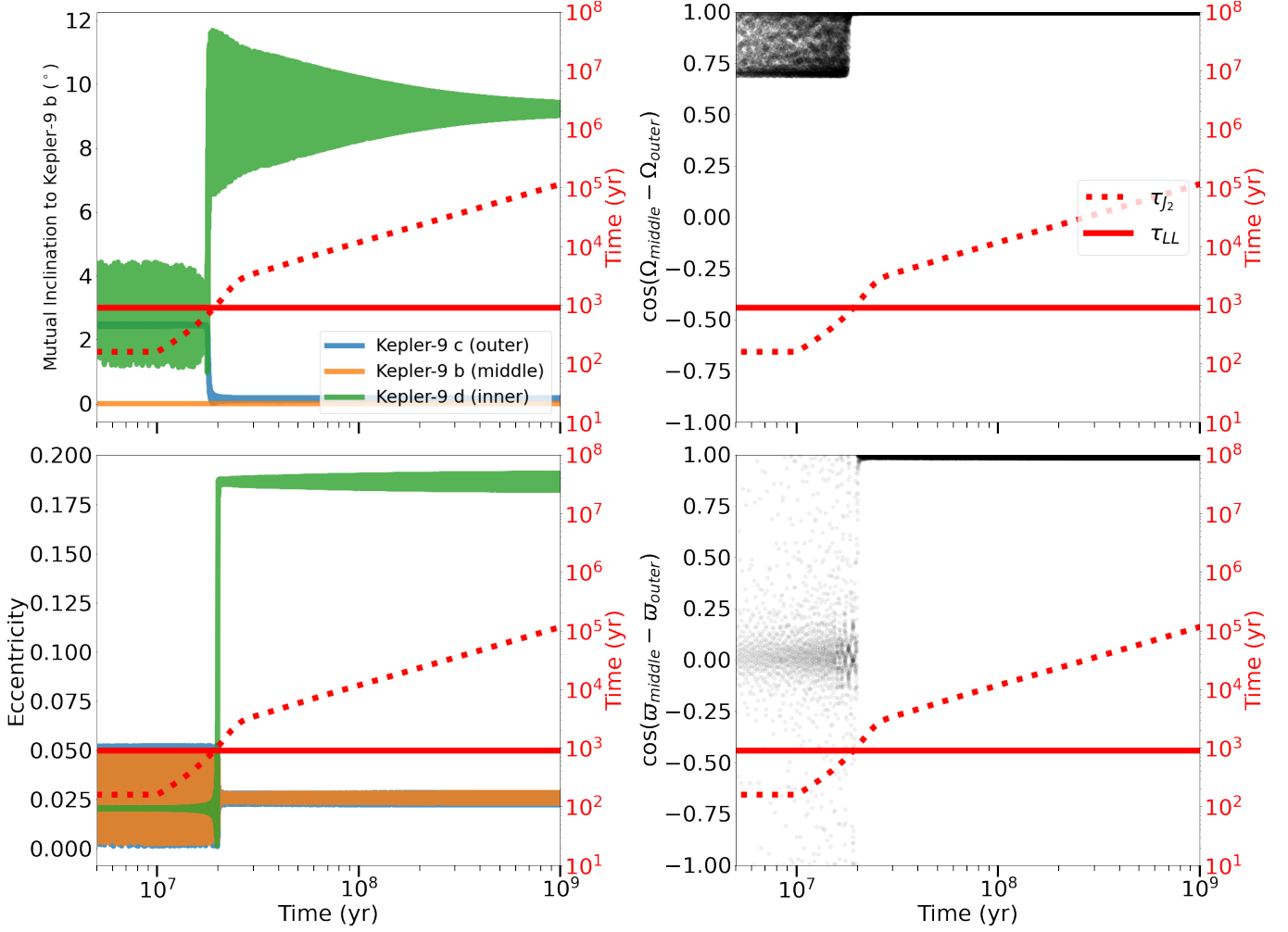


**Figure 3.** Time evolution of sun-like star Kepler-9’s planetary system. Upper Left: Mutual inclination between planets b, c, and d and Kepler-9 b (the middle planet) as a function of time. Lower Left: Eccentricity of Kepler 9 b, c, and d as a function of time. Upper Right: Evolution of the difference in longitudes of ascending node ( $\Omega$ ) between Kepler-9 b and c (the middle and outer planets) as a function of time. The alignment near  $2 \times 10^7$  years marks the resonance that misaligns Kepler-9 d from the rest of the planets, and simultaneously locks Kepler-9 b and c into coplanarity. Lower Right: Evolution of the difference in longitudes of periastris ( $\omega$ ) between Kepler-9 b and c as a function of time.

Overplotted on all figures are the precession timescales for  $J_2$  precession ( $\tau_{J_2}$ ) on the inner planet (dashed red lines), and Laplace-Lagrange (LL) precession on the inner planet ( $\tau_{LL}$ ) (approximated by  $A_{00} (= -B_{00})$ , solid red lines).

Object	Mass	Radius	$a$ (au)	$e^\dagger$	$i^\dagger$	$\Omega^\dagger$	$\omega^\dagger$	Reference
Star	$1.09 M_\odot$	$1.02 R_\odot$						Torres et al. (2011)
Kepler-9 d	<b><math>3.342 M_\oplus</math></b>	$1.64 R_\oplus$	0.0273	0.021	$0.57^\circ$	$1.61^\circ$	$89.5^\circ$	Torres et al. (2011)
Kepler-9 b	$43.4 M_\oplus$	$8.29 R_\oplus$	0.1437	0.026	$1.72^\circ$	$1.58^\circ$	$123.36^\circ$	Borsato et al. (2019)
Kepler-9 c	$29.9 M_\oplus$	$8.08 R_\oplus$	0.23015	0.045	$4.21^\circ$	$0.29^\circ$	$38.47^\circ$	Borsato et al. (2019)

**Table 1.** Initial conditions of Kepler-9 used in Figure 3. Bolded masses indicate masses calculated using the mass-radius relation shown in Müller et al. (2023). Semimajor axes are derived from periods rather than the associated references’ reported value to ensure the observed period ratios are maintained.  $^\dagger$ : parameters randomized according to the scheme described in Table 2.

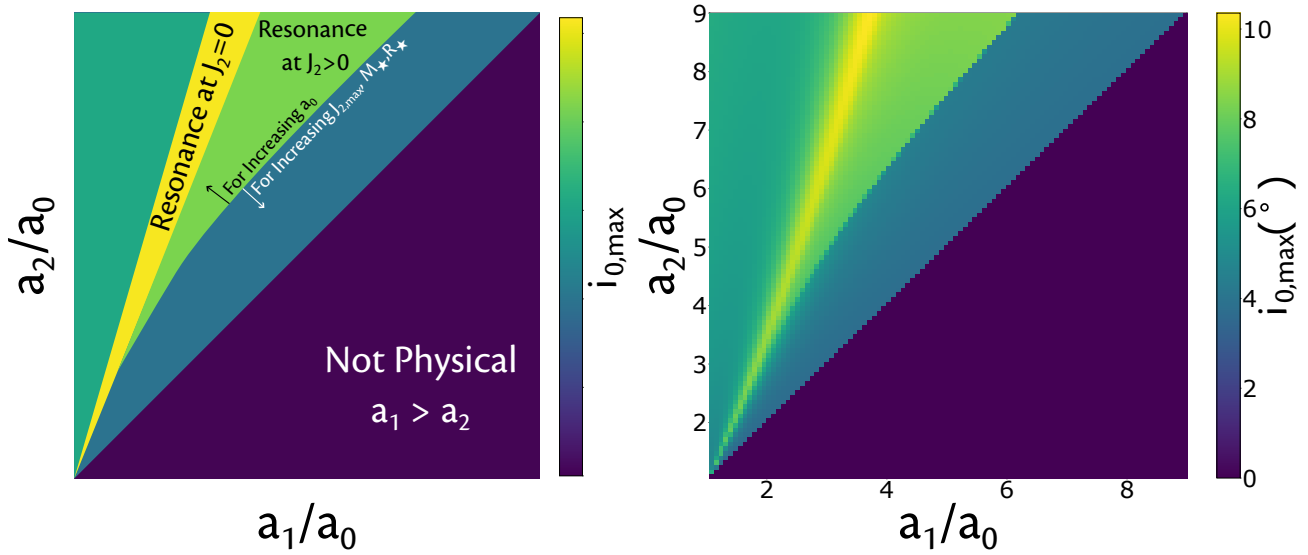


**Figure 4.** Left: Heuristic relationships between companion planet semimajor axis ratios (axes) and maximum inclination induced on the inner planet of a three planet system via planet-planet interactions (color bar) as  $J_2$  decreases over time. Annotations describe how variations of system parameters affect the structure. The boundaries between regions were drawn by eye as a representation of the right panel.

Right: Analytical calculation of relation between semimajor axis ratios and inner planet maximum inclination over all values of  $J_2$  explored by the star as it spins down.. The calculations were performed following the prescription described at the end of Section 2. Planets 1 and 2 were initialized with a  $3^\circ$  mutual inclination. Planet radii were selected as median radii in that orbital position across the 31 three-planet systems studied in Section 4 (i.e., the inner planet has the median radius of all inner planets in our sample of 3-planet systems (see Table 5), and so on for middle and outer planet). The inner planet was set at a semimajor axis of  $a_0 = 0.1$  au,  $J_2$  spanned from  $10^{-3} - 10^{-8}$ , and the inner, middle, and outer planet masses were set to 3.2, 9.2,  $12.3 M_\oplus$  respectively using the mass-radius relation of Müller et al. (2023).

across the parameter space. To the right of this region is a nonresonant region where  $a_1 \approx a_2$ . To the right of that region, indicated by the dark lower triangle, is a forbidden region by the restriction that  $a_2 > a_1$ . Written in the left panel are descriptions of how these regions’ boundaries change for different parameter values. For increasing  $a_0$ , the sweeping resonant region for  $J_2 > 0$  decreases in size, but the  $J_2 = 0$  resonance stays in place. For increasing maximum  $J_2$ ,  $M_*$ , and  $R_*$ , the sweeping resonant region for  $J_2 > 0$  increases in size.

The general shape shown in the right panel of Figure 4 is conserved across many choices of system parameters. Indeed, if  $J_2 = 0$ , there are no terms in Eqs (3)-(10) that depend on the individual semimajor axes of the planets—only the ratios between planets. Moreover, when  $J_2 = 0$ , assuming that  $m_j \ll M_*$  for all planets  $j$ , then scaling all the planet masses by the same amount will not affect the resulting inclination of the inner planet, as all elements of the matrices will be scaled by the same amount—keeping the eigenvectors constant. However, relaxing  $J_2 = 0$  can turn on the “Sweeping Resonance” region. In this case, scaling up all the planet masses reduces the magnitude of the precession caused by  $J_2$  compared to planet-planet interactions. This weakening pushes the region where the inner planet experiences “Sweeping Resonances” to larger values of  $a_1$  and  $a_2$ , where the mass-boosted planet-planet interactions no longer dominate the  $J_2$  precession.

The effect of the planet masses can also be mapped out like we have for the semimajor axes. In Figure 5, we show the impact of varying the ratios between the outer planets’ masses and the inner planet’s mass for four different sets of semimajor axes. As a base system, we use the characteristic parameters shown in the right panel of Figure 4. The four choices of semimajor axis ratios are labeled on the left panel of Figure 5, and feature fixed outer and inner planet semimajor axes, with a varying middle planet semimajor axis between them. The middle planet’s semimajor axis is varied such that the system explores the four regimes: nonresonant with a small middle planet semimajor axis (labeled ‘A’), static resonance (labeled ‘B’), sweeping resonance (labeled ‘C’), and nonresonant with a large middle planet semimajor axis (labeled ‘D’). The green stars indicate the masses that were used when calculating the left side of Figure 5. In region ‘A,’ the nonresonant region, the relationships between mass and inclination induced are smooth, with a slightly larger inclination achieved when  $m_2$  increases and  $m_1$  stays the same. In region ‘B,’ the effect of resonance is made clear by the vastly enhanced inclination when both masses  $m_1$  and  $m_2$  increase relative to  $m_{in}$ . In region ‘C,’ the sweeping resonance re-

gion, the figure shows the range of masses that allow for sweeping resonance. For  $0 < \log_{10}(m_1/m_{in}) < 1.25$  and  $-1 < \log_{10}(m_2/m_{in}) < 1$ , there is a wedge of parameter space with enhanced inclination. Outside this wedge, the induced inclination is similar to region ‘A,’ the nonresonant region, indicating that for those masses, no sweeping resonance exists. Region ‘D’ appears similar to region ‘A,’ which is fitting as they are both nonresonant; however, at smaller values of  $m_1$  and  $m_2$ , a similar wedge shape to region ‘C’ appears. This indicates that for choices of masses that lie within that wedge, there would be a sweeping resonance at the semimajor axis ratios denoted by region ‘D.’

Notable in Figure 5 is the effect of increasing companion planet masses. In the resonant regions (panels ‘B’ and ‘C’), increasing the masses of the outer planets relative to the innermost planet (i.e., moving the green star upward and rightward) tends to increase the amount of misalignment produced by the resonances. However, especially in panel ‘C,’ this is not guaranteed. If the masses of the outer two planets are increased past a certain point, then the strength of  $J_2$  precession relative to the precession caused by planet-planet interactions decreases, and the requisite  $J_2$  to push the inner planet into resonance is higher than the maximum  $J_2$  allowed. This defines the top edge of the wedge shape in panel ‘C.’ Unlike region ‘C,’ in region ‘B’ where  $J_2 = 0$ , there is no maximum outer planet masses beyond which no resonance occurs. The green strip extending to high mass ratios indicates that for a large, given outer planet mass, a middle planet mass exists that brings the inner planet into resonance. A similar phenomenon is also shown in panel ‘A.’ If, from the mass ratios of the green star,  $m_2/m_0$  is increased and  $m_1/m_0$  is held constant, then the system can enter the resonant region visible above the green star. In this sense, region ‘A’ is not truly non-resonant for all planet masses.

#### 4. OBSERVED SYSTEMS

Clearly, sweeping secular resonances can have significant impact on exoplanet systems. This naturally poses the question: to what extent are these effects reflected in the known exoplanet sample? To investigate this, we consider 31 known exoplanet systems. These systems were selected from the NASA Exoplanet Archive (NASA Exoplanet Science Institute 2024) with the following criteria: **1)** The host star has its temperature in the range for FGK-type stars below the Kraft break; **2)** The host star has its mass and radius measured and is not significantly evolved; **3)** The planetary system has exactly three observed planets; **4)** Each planet in the system transits its host star; and **5)** Each planet in the

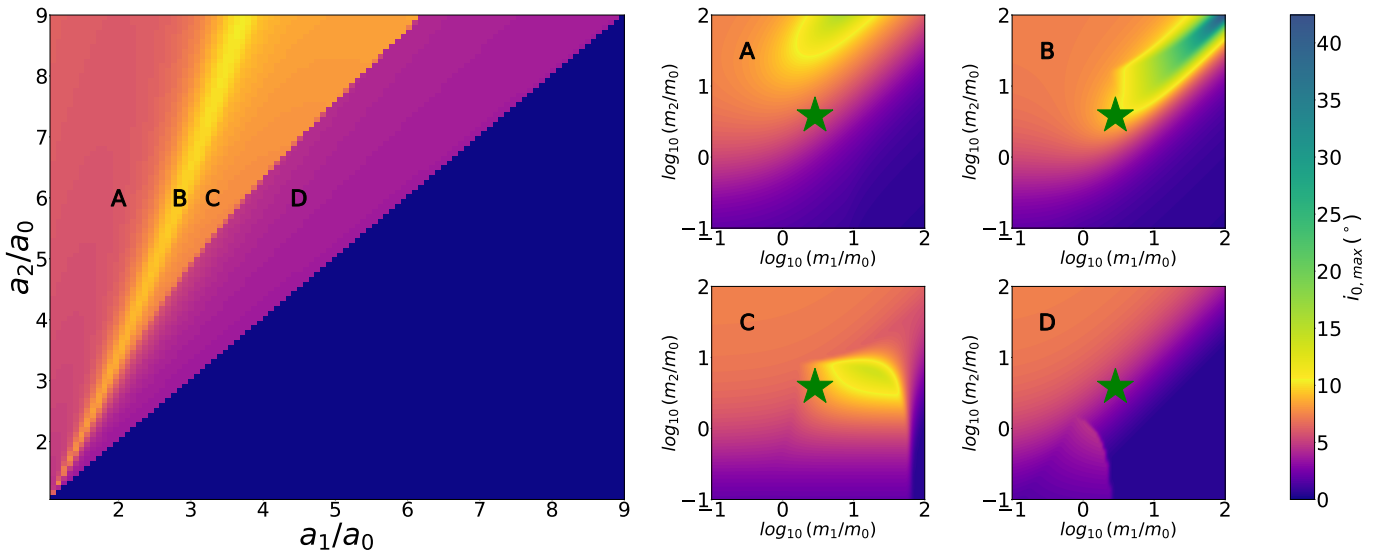


**Figure 5.** Left: Relationship between companion planet semimajor axis ratios (axes) and maximum inclination induced on candidate inner planet via resonance (color bar). Planets 1 and 2 were initialized with a  $4^\circ$  mutual inclination. Right: Effects of the variation of the masses of the outer two planets at four different sets of semimajor axis ratios shown on the leftmost panel corresponding to the four different qualitative regions shown: A)  $a_{in}$  and  $a_1$  are too close and  $a_2$  too far away for the system to enter resonance; B)  $a_1$  and  $a_2$  are such that the inner planet is in resonance with the outer two at  $J_2 = 0$ ; C)  $a_1$  and  $a_2$  are such that the inner planet is in resonance with the outer two for some particular  $J_2 \neq 0$ ; D)  $a_1$  and  $a_2$  are such that the inner planet will never be in resonance with the outer two for any of the  $J_2$  values the star will explore. The green stars mark the mass ratio assumed in the left panel.

system has its mass or its radius measured. After all five criteria have been applied, only 31 systems remain. In cases where a planet only had its radius measured, its mass was assigned by the Mass-Radius relation given in Müller et al. (2023). The parameters adopted are listed in Table 5.

To quantify which systems undergo systematic misalignments similar to those depicted in Figure 3, for each of these 31 systems, we run 100 integrations of the secular equations described in Eqs 11. In these integrations, we include the effects of precession due to  $J_2$  and GR, and we let  $J_2$  evolve according to the upper curve of Figure 2. Each simulation was allowed to run for 2 Gyr. In each simulation the initial conditions of the planets were randomized according to the prescription given in Table 2. We find that six of these 31 systems exhibit permanent misalignments between planets mediated by  $J_2$ . Similar to the evolution depicted in Figure 3, when  $J_2$  passes a critical value, the outer two planets in these systems align their orbits. Simultaneously, the innermost planet becomes misaligned from the outer two. The values of  $J_2$  and the corresponding times when the misalignment occurs are listed in Table 3.

In Figure 6, we show the structure in  $a_1/a_0$ - $a_2/a_0$  space of nine systems. Each panel of Figure 6 represents a different observed system, with the observed values of the semimajor axis ratios (derived from the extremely accurately measured period ratios) marked with a red

dot. The top two rows of Figure 6 are the six systems from our 31-system sample which were found in the Monte Carlo simulations to undergo permanent misalignments. The bottom row of Figure 6 contains three of the 25 systems whose simulations did not undergo permanent misalignments. The bottom row systems are chosen from various regions of non-sweeping parameter space: high  $a_1/a_0$  (Kepler-616; see Table 5), “static” resonance that does not sweep, and therefore does not produce misalignments (TOI-2076; discussed in detail in Section 4.2), and low  $a_1/a_0$  (HD 22946; see Table 5).

To quantify the misalignment present in a system caused by changing  $J_2$ , we define the parameter

$$\Delta i_{jk}^{mut} = \langle i_{jk}^{mut} \rangle_{late} - \langle i_{jk}^{mut} \rangle_{early} , \quad (18)$$

where  $\langle i_{jk}^{mut} \rangle_{early}$  is the time-averaged mutual inclination between planets  $j$  and  $k$  before  $t = 1$  Myr (this is before  $J_2$  evolution is turned on at  $t = 10$  Myr) and  $\langle i_{jk}^{mut} \rangle_{late}$  is the average mutual inclination between planets  $j$  and  $k$  during the last 40 Myr of the simulation. A positive value of  $\Delta i_{jk}^{mut}$  implies that planets  $j$  and  $k$  became more misaligned over the course of the simulation, and a negative value implies that planets  $j$  and  $k$  aligned themselves. We choose to define  $\Delta i_{jk}^{mut}$  in terms of time-averages at early and late times to remove dependence on the initial phase of inclination oscillation.

In each panel of Figure 7, we show the relationship between the initial mutual inclination between the outer

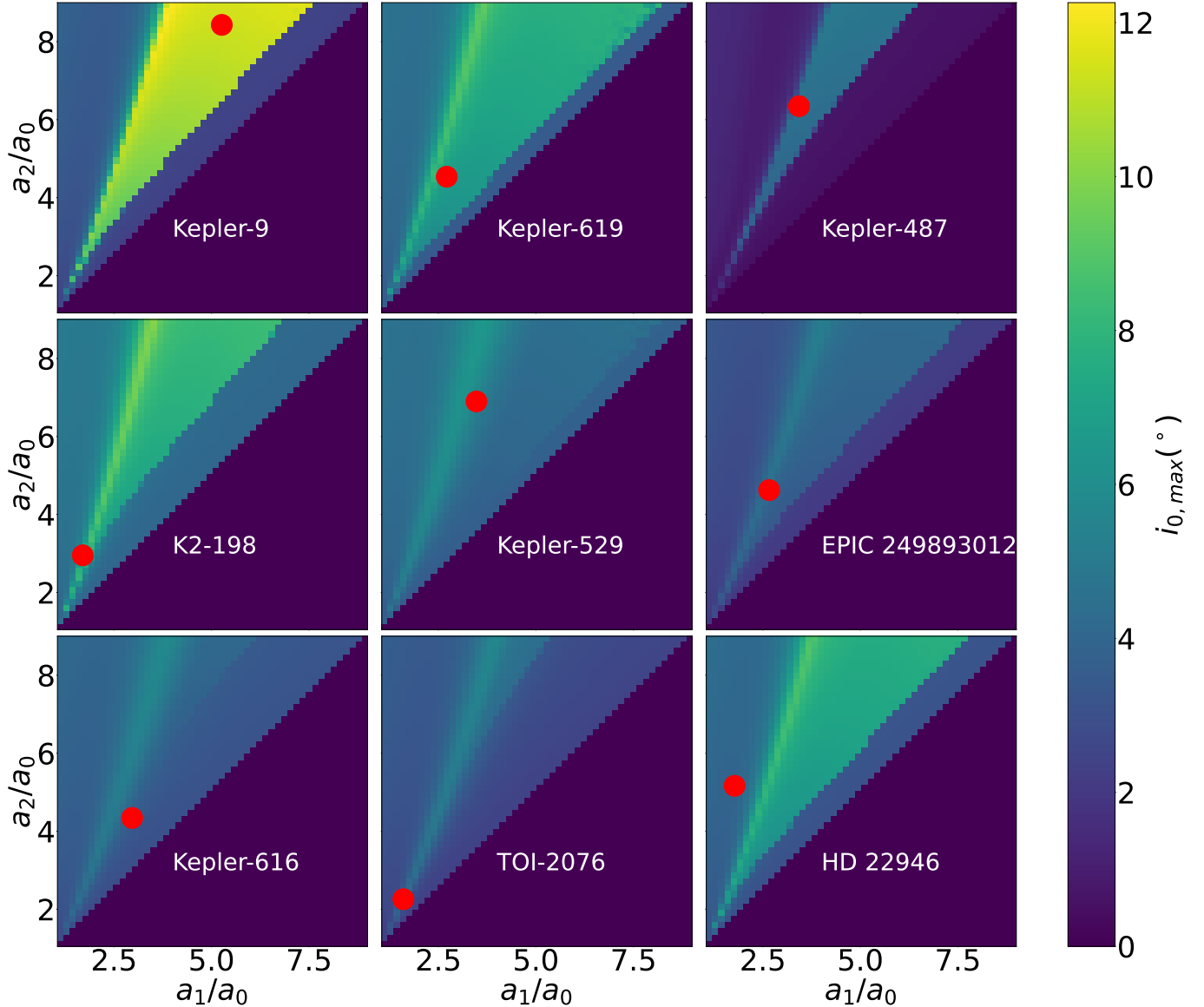


**Figure 6.** Relation between companion semimajor axes and inner planet maximum inclination for nine of the 31 identified three-planet systems in our sample. The initial mutual inclination between the outer planets for each panel was set to  $3^\circ$ . The top two rows contain only systems that undergo sweeping resonances, and the bottom row contains only systems that do not.

Object	Mass, Stellar Radius	$a$ (au)	$e$	$i$	$\Omega$	$\omega$
Star	From Reference					
Inner Planet	From Reference	From Reference	$\mathcal{R}(0.049)$	$1^\circ$	$\mathcal{U}(2\pi)$	$\mathcal{U}(2\pi)$
Middle Planet	From Reference	From Reference	$\mathcal{R}(0.049)$	$\mathcal{R}(0.049 \text{ rad})$	$\mathcal{U}(2\pi)$	$\mathcal{U}(2\pi)$
Outer Planet	From Reference	From Reference	$\mathcal{R}(0.049)$	$\mathcal{R}(0.049 \text{ rad})$	$\mathcal{U}(2\pi)$	$\mathcal{U}(2\pi)$

**Table 2.** Randomization Scheme for Simulations. Simulations were integrated for 2 Gyr.  $\mathcal{R}(\sigma)$  represents a random variable drawn from a Rayleigh distribution with scale  $\sigma$ .  $\mathcal{U}(X)$  represents a random variable drawn from a uniform distribution between 0 and  $X$ .

System	Resonant $J_2$	$t_{res}$ (yr)
Kepler-9	$1.3 \times 10^{-4}$	$1.7 \times 10^7$
Kepler-619	$7 \times 10^{-5}$	$2 \times 10^7$
Kepler-487	$1.1 \times 10^{-4}$	$1.85 \times 10^7$
K2-198	$8.3 \times 10^{-5}$	$2 \times 10^7$
Kepler-529	$1.8 \times 10^{-5}$	$4.6 \times 10^7$
EPIC 249893012	$2.1 \times 10^{-4}$	$1.5 \times 10^7$

**Table 3.** Values of  $J_2$  for system inclination resonance for the six sweeping-resonant systems identified in Section 4. Additionally, the corresponding times for this  $J_2$  value are listed (following the top curve of Figure 2).

two planets (x-axis) and the change in planets’ relative alignment (y-axis,  $\Delta i_{01}^{mut}$  in red and  $\Delta i_{12}^{mut}$  in blue). The top two rows are systems whose positions in  $a_1/a_0$ – $a_2/a_0$  space indicate they undergo sweeping resonances. For these systems, there is an approximately linear relationship between initial mutual inclination between outer planets, and the (mis-)alignments between the planets after  $J_2$  evolution has had its effect. In each panel, the dotted red line represents the minimum mutual inclination between the middle and inner planets such that the inner planet may not co-transit with the middle planet (under the simplifying assumption that the middle planet’s transit impact parameter  $b = 0$ ). Many of the sweeping resonant systems would require very large initial mutual inclinations between the outer two planets to make the inner planet no longer transit.

However, that is not the only constraint we can place on the initial conditions. If the outer two planets are prepared with high initial mutual inclinations, under what conditions do they align enough over the course of the simulation such that at the end, they both transit? This is shown in the black dotted lines. For blue triangles above the black dotted line, the initial mutual inclination between the outer two planets is too high for them to transit together (assuming the middle planet’s impact parameter  $b = 0$ ), even after the sweeping resonance from evolving  $J_2$  partially aligns their orbits. For example, even though the inner planet of K2-198 still transits with the middle planet even for high  $i_{mut,12,init}$ , the outer two planets do not align enough from sweeping resonances to overcome any  $i_{mut,12,init} \gtrsim 2^\circ$ . On the other hand, even if  $i_{mut,12,init}$  is set to  $10^\circ$  in Kepler-9 or Kepler-619, the outer planets always align enough from the sweeping resonance to co-transit.

#### 4.1. Sweeping Resonant Systems

In Figure 6 we showed six systems that lie in the range of parameter space where sweeping resonances via  $J_2$  evolution can occur. Parameters adopted for all 31 systems in the sample are shown in Table 5. Below we com-

ment on Kepler-9 and EPIC 249893012, as their properties are of note.

##### 4.1.1. Kepler-9

Kepler-9 is a well-studied system, discovered by Holman et al. (2010). As it was one of the first-validated Kepler systems, its parameters have been studied and adjusted many times through transits, transit timing variations, and radial velocity measurements (e.g., Borsato et al. 2019; Albrecht et al. 2021; Berger et al. 2018; Wang et al. 2018; Hadden & Lithwick 2017; Holczer et al. 2016; Morton et al. 2016; Borsato et al. 2014; Hadden & Lithwick 2014; Torres et al. 2011; Weiss et al. 2024). The outer two planets are near, but outside, a 2 : 1 mean-motion resonance that integrations of the most recent fits indicate is an unstable resonance (e.g., Antoniadou & Libert 2020). The literature suggests that the outer two planets have aligned orbital axes (e.g., Freudenthal et al. 2018), which we note is consistent with the damping out of any primordial orbital misalignments between them as shown in Figures 3 and 7.

##### 4.1.2. EPIC 249893012

EPIC 249893012 is a sun-like star just beginning its evolution off the main sequence (Hidalgo et al. 2020). As it is no longer a main-sequence star, it would normally have been excluded from this sample. However, as there is substantial evidence this star is just leaving the main sequence, its mass while its  $J_2$  was spinning down would have been approximately the same as its current mass and therefore the planets should not have experienced stellar evolution-based migration. Therefore, it is a valid inclusion, and for the purposes of this work, we have set its radius to  $1.1 R_\odot$ .

Gupta & Schlichting (2021) calculates that the inner planet, EPIC 249893012 b, is losing mass at a rate of approximately  $10^8 g/s$ . However, if this mass loss rate has been sustained for the entire age of the system  $\sim 9$  Gyr, the mass of EPIC 249893012 b would have changed by only  $0.005 M_\oplus$  since its formation. Therefore, we adopted EPIC 249893012 b’s currently measured mass for use in our simulations, as its atmospheric mass loss does not alter significantly its total mass.

#### 4.2. The Impact of Static vs Sweeping Resonances

As depicted in Figure 4, we identify a region in resonance associated with  $J_2 = 0$  (the yellow strip, labeled “Resonance at  $J_2 = 0$ ”). Not all of this  $J_2 = 0$  resonant region produces systematic misalignments similar to those demonstrated in Figure 3. At small values of  $a_1/a_0$  and  $a_2/a_0$  or when  $a_0$  is large, or both, the precession rate caused by  $J_2$  is slow (even at  $J_2 = 10^{-3}$ ) compared to the precession caused by planet-planet interac-

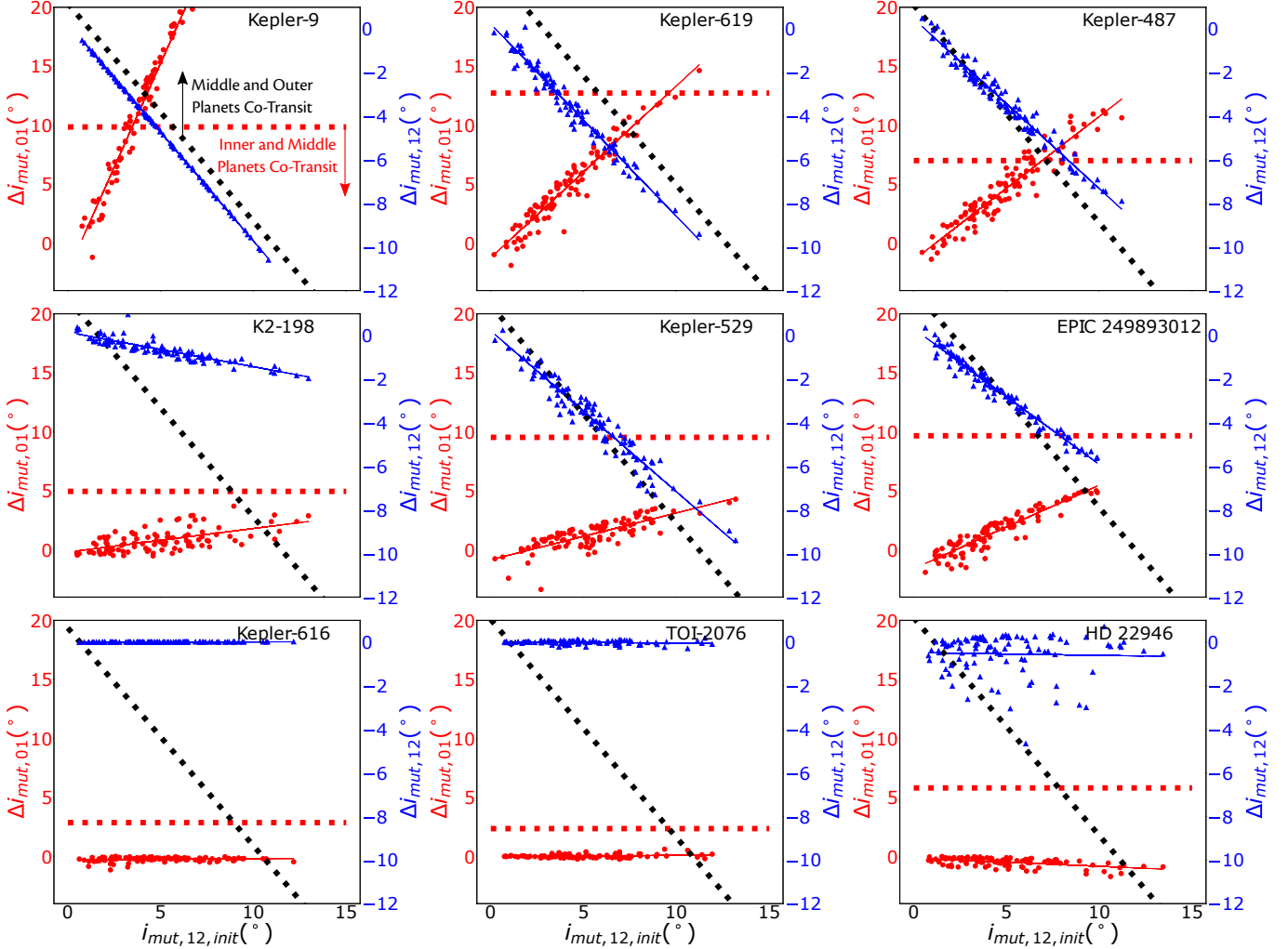


**Figure 7.** Relation between initial mutual inclination between the two outermost planets and changes in alignment between planets over the course of the simulation for nine systems. The top six systems undergo resonance-mediated misalignments. The bottom three do not. In red circles are, for each simulation, the change in alignment between the inner and middle planets—the average mutual inclination at late times between the inner and middle planet minus the initial mutual inclination between the inner and middle planet. The red dotted line represents the minimum  $\Delta i_{mut,01}$  such that the inner planet fails to transit at the end of the simulation (under the simplifying assumption that the middle planet has a transit impact parameter  $b = 0$ ). In blue triangles are, for each simulation, the change in alignment between the middle and outer planets—the average mutual inclination at late times between the middle and outer planet minus the initial mutual inclination between the middle and outer planet. The black dotted line represents the maximum value of  $\Delta i_{mut,12}$  as a function of  $i_{mut,12,init}$  such that the outer two planets both transit at the end of the simulation. The scheme by which orbital parameters were varied between simulations is described in Table 2.

tions. In this case,  $J_2$  precession is not fast enough to shift the location of the secular resonance for any value of  $J_2$  the star can be reasonably expected to achieve. We call these unmoving resonances “static”.

Static resonances notably do not produce the misalignment from evolving  $J_2$  that sweeping resonances do. For example, the system TOI-2076 (observed by e.g., Osborn et al. 2022; Hedges et al. 2021) lies on such a static resonance as depicted in the bottom middle panel of Figure 6. In Figure 9, we show the semimajor axis parameter space of TOI-2076 for  $J_2 = 10^{-3}$  (left panel)

and  $J_2 = 0$  (right panel). The location of TOI-2076’s observed semimajor axis ratios is marked with a red dot. In both panels, TOI-2076 lies on a secular resonance with the same expected inner planet maximum inclination. This indicates that there is no expected change to the system as  $J_2$  evolves from  $\sim 10^{-3}$  to 0. Therefore, we do not expect the inner planet to systematically and/or permanently misalign from its companions any more than is provided in its initial conditions.

Indeed, in Figure 8, we show the time evolution of one of the simulations of TOI-2076 from the Monte Carlo.

In the bottom left panel, we can see that the longitudes of ascending nodes between the outer two planets are locked together, indicating the resonance is active; however, the upper left panel shows that mutual inclinations do not significantly change. The planets do not misalign. In the bottom middle panel of Figure 7, we can see that even for large initial values of  $i_{mut,12}$ , no permanent misalignment occurs between the planets in this system—they retain whatever mutual inclinations they are initialized with.

Therefore, the misalignments shown in the sweeping resonant systems depicted in the top two rows of Figure 7 arise because these systems are initially not in resonance for high  $J_2$  values, then enter resonance as  $J_2$  decreases, increasing the inner planet’s inclination predicted from Laplace-Lagrange. Depending on their locations in  $a_1/a_0$ – $a_2/a_0$  space, the planets may later leave resonance, but the mark of having passed through resonance is left on their mutual inclinations. It is the change/increase in predicted inclinations from Laplace-Lagrange due to evolving  $J_2$  that produces the misalignments.

## 5. DISCUSSION

Out of our clean sample of 31 three-planet transiting systems, we found six systems whose parameters indicate they may have undergone sweeping resonance during their first Gyr due to  $J_2$  evolution. This corresponds to one system in five, or  $\sim 20\%$ , indicating that the architectures that produce these misalignments may be common. While performing a full completeness analysis to estimate the true number of systems with these architectures is beyond the scope of this work, below, we identify some considerations that may affect the true value of the 1 in 5 number if accounted for.

1. Closer-orbiting planets are more sensitive to  $J_2$  sweeping resonances than further-orbiting planets. Because closer-orbiting planets are easier to detect via transit, systems with closer-orbiting planets will be overrepresented in the transit catalogue compared to the true, underlying distribution. Accounting for this would decrease the 1 in 5 rate.
2. Three-planet systems seem ubiquitous in our Galaxy, with an estimated 30% of sun-like stars hosting a system of  $\sim 3$  planets with sub-400 day periods (Zhu et al. 2018). As this is an expected value, higher multiplicity systems are also likely and have been detected (for example, the 7-planet TRAPPIST-1 system (Gillon et al. 2016) or the 8-planet Kepler-90 system (e.g., Cabrera et al. 2014; Shallue & Vanderburg 2018)). A larger number

of planets in a system increases the possibility of a resonance, and finding previously undetected planets in observed systems is a common occurrence. Therefore, some three-planet systems may be four-planet systems or higher. Accounting for this would increase the 1 in 5 rate.

3. Our sample of 31 systems only includes systems where all three planets transit. This biases our sample towards systems that have low present-day mutual inclinations. Any system that was sufficiently misaligned by evolving  $J_2$  from a transiting configuration such that it does not transit today could never be included in our sample. In other words, our selection criteria can only produce systems where the induced misalignments are low enough for the planets to remain transiting. Accounting for this would increase the 1 in 5 rate.
4. In our calculations we adopted the upper estimate of the  $J_2$  evolution depicted in Figure 2. Not all stars will be born on the upper end of the initial spin distribution, and thus some systems may not undergo sweeping resonance that they might otherwise experience if the host star was born spinning faster. Accounting for this would reduce the 1 in 5 rate.

The third consideration naturally prompts the following questions. Shouldn’t the sweeping resonant systems we found have misaligned themselves out of their co-transiting configurations? Is it surprising that as many systems as we found lie within the sweeping resonance region that misaligns orbits? As an example, consider the Kepler-9 system. Kepler-9 d, the inner planet, orbits with  $a/R_\star = 5.54$ . Assuming for simplicity that the outer two planets have transit impact parameters of 0, then Kepler-9 d would need a mutual inclination of over  $\arctan(R_\star/a) \approx 10^\circ$  with the outer planets in order to escape transit. Figure 7 indicates that to become that inclined, the initial mutual inclination between the outer planets would have to be  $\sim 4^\circ$  or greater. The distribution of mutual inclinations for observed co-transiting planets is well-modeled by a Rayleigh Distribution with  $\sigma = 1^\circ - 2^\circ$  (see e.g., Fang & Margot 2012; Fabrycky et al. 2014). If the true distribution of initial mutual inclinations is similar to this model, it makes sense that Kepler-9 d still transits today. Even though it has likely been misaligned from its companions via  $J_2$  sweeping resonances, it would require an initial mutual inclination between outer planets of  $\sim 4^\circ$  to prevent the inner planet from transiting (see Figure 7). Of the systems we found, Kepler-9 is the most easily inclined, so for none

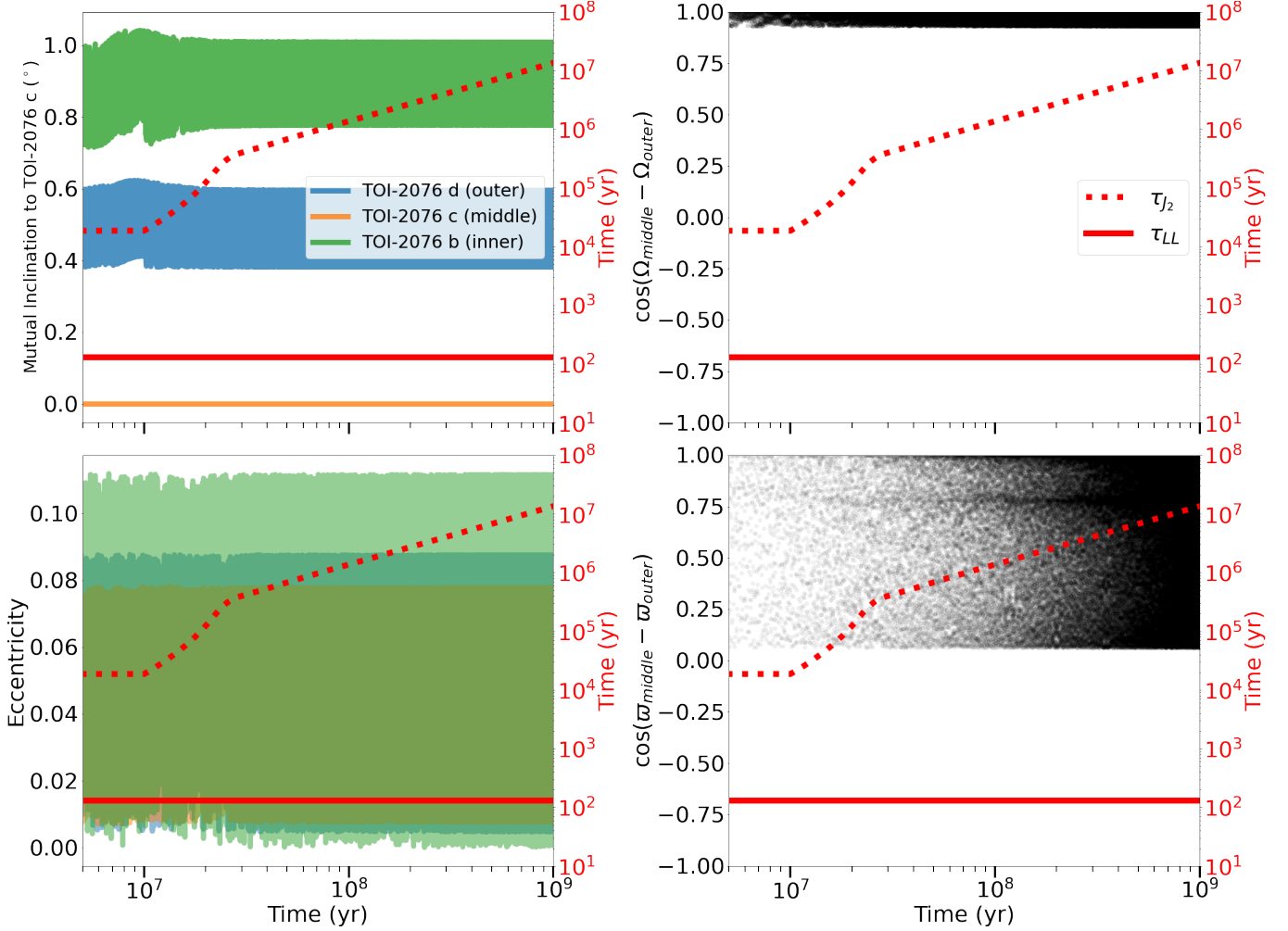


**Figure 8.** Time evolution of K-star TOI-2076’s planetary system. Upper Left: Mutual inclination between planets b, c, and d and TOI-2076 c as a function of time. Lower Left: Eccentricity of TOI-2076 b, c, and d as a function of time. Upper Right: Evolution of the difference in longitudes of ascending node ( $\Omega$ ) between TOI-2076 c and d (the middle and outer planets) as a function of time. Lower Right: Evolution of the difference in longitudes of periastris ( $\omega$ ) between TOI-2076 c and d as a function of time.

Overplotted on all figures are the precession timescales for  $J_2$  precession on the inner planet, and Laplace-Lagrange (LL) precession on the inner planet (approximated by  $A_{00} = -B_{00}$ ).

Object	Mass	Radius	$a$ (au)	$e^\dagger$	$i^\dagger$	$\Omega^\dagger$	$\omega^\dagger$	Reference
TOI-2076	$0.82 M_\odot$	$0.77 R_\odot$						Osborn et al. (2022)
TOI-2076 b	<b><math>10.4 M_\oplus</math></b>	$2.51 R_\oplus$	<b>0.087</b>	0.032	$0.57^\circ$	$1.25^\circ$	$107.5^\circ$	Osborn et al. (2022)
TOI-2076 c	<b><math>17.2 M_\oplus</math></b>	$3.50 R_\oplus$	<b>0.139</b>	0.066	$1.61^\circ$	$1.24^\circ$	$281.4^\circ$	Osborn et al. (2022)
TOI-2076 d	<b><math>15.2 M_\oplus</math></b>	$3.23 R_\oplus$	<b>0.196</b>	0.057	$2.03^\circ$	$1.7^\circ$	$318.2^\circ$	Osborn et al. (2022)

**Table 4.** Initial conditions of TOI-2076 used in Figure 8. Bolded masses indicate masses calculated using the mass-radius relation shown in Müller et al. (2023). Bolded semimajor axes indicate semimajor axes calculated from stellar mass and planetary orbital period.  $^\dagger$ : parameters randomized according to the scheme described in Table 2.

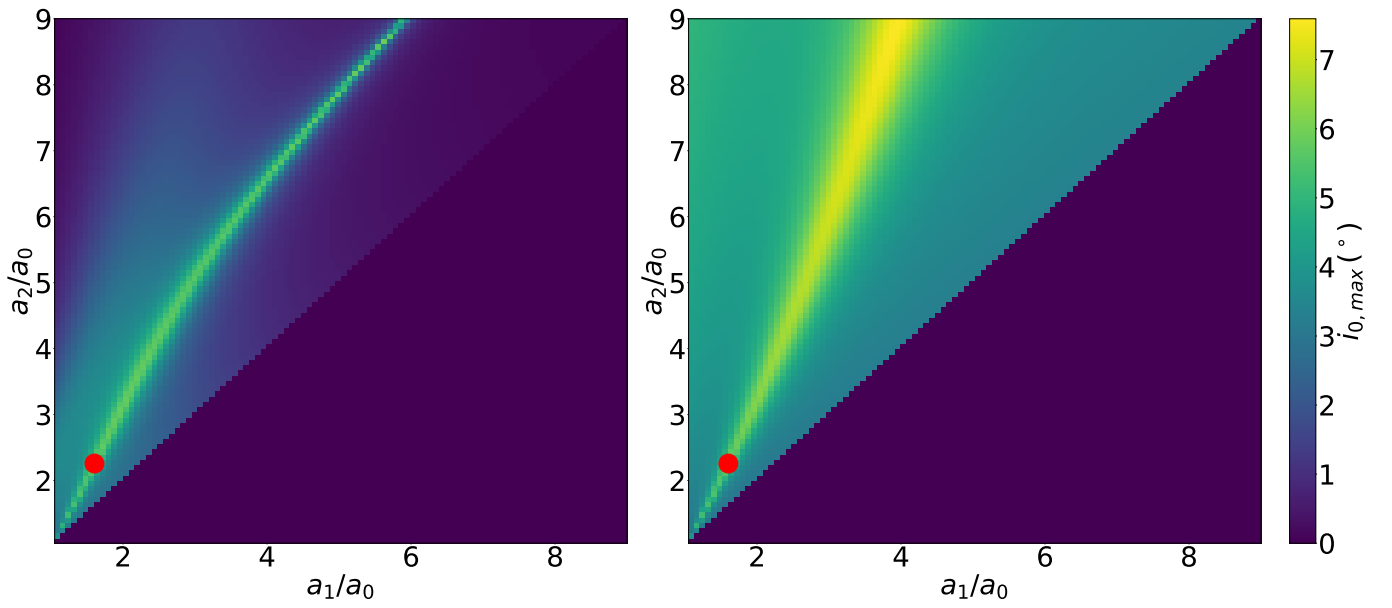


**Figure 9.** Parameter space of TOI-2076 with  $J_2$  fixed at  $10^{-3}$  (left panel) and 0 (right panel). The observed locations of the outer planets are shown by a red dot. The mutual inclination between the outer two planets of TOI-2076 was set to  $3^\circ$ .

of the systems identified is it particularly surprising that all three planets transit.

This naturally brings to mind the possibility of systems where the inner planet is so greatly misaligned from its companions that it no longer transits. These systems would likely present as two-planet transiting systems, as the outer planets align as a consequence of misaligning the inner (see the negative slopes of the blue curves in Figure 7). However, two effects add together to potentially limit the occurrence rate of such systems: 1) high required mass ratios and 2) configurational restrictions. The first effect is relatively simple: the higher the mass ratio between the inner and outer planets, the more misalignment is produced. For example, the mass ratio between Kepler-9’s inner and middle planets is  $\sim 5$ , which enables the steep slope of  $\Delta i_{01}^{mut}$  with respect to  $i_{mut,12,init}$ . While a mass-ratio of 5 is relatively small compared to the  $\sim 300$  between Earth and Jupiter, mass ratios in observed, compact, multi-transiting systems tend to be relatively small (e.g., Weiss et al. 2018).

The second effect limiting how often systems can be misaligned out of transit is configurational. As mentioned, further-orbiting inner planets require less misalignment in order to escape transit. But the minimum semimajor axis ratios for sweeping resonance to occur increase as the inner planet is further from the host star. This is because sweeping resonance requires commensurability in magnitude between planet-planet precession and  $J_2$  precession, which can’t happen if all planets are far from the star, but close to one another. This means that the further the inner planet orbits from the star, the larger the semimajor axis ratios between the middle and outer planets and the inner planet need to be (see for example the difference in sweeping resonance locations for Kepler-619 compared to Kepler-616 in Figure 6). The further the inner planet orbits, the more physically isolated it must be from its companions in order to experience sweeping resonance, and such systems don’t appear to be common.

The impact of sweeping resonances via  $J_2$  also poses an interesting possibility. The size of the sweeping region in semimajor axis ratio space (see Figure 6) depends on the maximum value of  $J_2$  that the star experiences. This means that the present-day mutual inclinations between planets depend on the maximum  $J_2$  achieved, meaning that the maximum spin of the star (and therefore the maximum  $J_2$ ) could be constrained by present-day planetary configurations. Because stellar spins as functions of time tend to be relatively indistinguishable after  $\sim 1$  Gyr regardless of initial spin (see, e.g., Barnes 2003; Hartman et al. 2010; Delorme et al.

2011; Meibom et al. 2015), this dynamical channel could provide a way to probe the initial conditions of billions of years-old stars. Simultaneously, the trends in Figure 7 show a remarkable dependence between mean mutual inclination at late times and initial mutual inclination. This relationship may allow some constraints to also be put on the maximum mutual inclination between outer planets during the early years of the system’s life—when  $J_2$  was moving through its high values that drive the resonances. A straightforward implementation of this is present in Figure 7, represented by the black dotted line: blue dots above this line should not present as co-transiting systems and are thus forbidden.

We note that if a system has parameters today that lie within the sweeping resonance region, that is not a guarantee that it actually underwent sweeping resonance in its past. One potential concern is whether the true stellar mass or radius deviates significantly from the values in the literature—it is noted in Figure 1 that both  $M_\star$  and  $R_\star$  affect where the sweeping resonance lies. Moreover, if  $J_2$  decrease begins earlier than we assume, the disk may still be present and the planets may still be migrating, meaning that the starting  $J_2$  of the post-migration epoch would be lower. We discuss this possibility in detail in Appendix B. We explore observed systems to indicate how common sweeping-resonant architectures may be rather than attempting to claim with certainty which of these 31 systems did or did not undergo sweeping resonance via  $J_2$ . Making such claims is possible; however, we do not do so here.

## 6. CONCLUSION

In this work, we explored the implications of the evolution of stellar oblateness ( $J_2$ ) on systems of multiple planets during the first Gyr, showing that  $J_2$  evolution can bring nonresonant systems into and out of secular resonance (“sweeping resonance”). While sweeping resonances were pointed out before in the context of  $J_2$  in multi-planet systems (e.g., Brefka & Becker 2021; Faridani et al. 2023; Spalding et al. 2018), here we focus on the implications for observed systems.

As a case study, we focus on three-planet systems. As time goes by, magnetic braking slows the spin of the star, reducing  $J_2$ . A three-planet system, initially not in resonance, can be captured in a Laplace-Lagrange resonance at a certain  $J_2$ . If the inner planet is as-massive or less-massive than its companions, the mutual inclination between the outer two planets is damped out as the system enters resonance. In that case, the mutual inclination between the outer pair and the inner planet increases to conserve angular momentum. This can pro-

duce large mutual inclinations between the inner planet and the outer pair.

Whether or not sweeping resonances from  $J_2$  occur at all depends on the semimajor axes and masses of the planets. In Figure 4, we show the relationship between the semimajor axis ratios in the system and the subsequent inclination induced on the inner planet by sweeping resonances from evolving  $J_2$ . A large portion of the parameter space exhibits sweeping resonances when  $a_1/a_0$  and  $a_2/a_0$  are both large—a much larger portion of the space than is produced without evolving  $J_2$ . Similarly, when  $a_0$  decreases, the rate of  $J_2$  precession increases relative to planet-planet precession, so more of the parameter space exhibits sweeping resonances when  $a_0$  is small. The mass ratios between the planets also affect where the resonances are located, but the sensitivity is small, with mass changes up to a factor of 2 or 3 not necessarily affecting whether a system enters resonance.

To determine how common sweeping resonances from evolving  $J_2$  are, we explored the population of observed, three-planet systems. We found that  $\sim 20\%$  of a sample of three-planet all-transiting systems have mass and semimajor axis ratios that indicate they underwent sweeping resonances early in their lives. In Fig-

ure 7, we show that the ability of sweeping resonances to misalign the inner planet from its companions is dependent on the initial mutual inclination between the outer two planets. Moreover, for all six sweeping-resonant systems we identified, they would require very large outer planet mutual inclinations to make the inner, transiting planet no longer transit-consistent with observations. Our findings have significant implications for the connection between exoplanet systems’ initial conditions and their present configurations. A fraction of systems experiencing sweeping resonances of near 20% constitutes a generic, ubiquitous phenomenon.

#### ACKNOWLEDGEMENTS

The authors would like to thank Songhu Wang for useful discussions. This research has made use of the [NASA Exoplanet Science Institute \(2024\)](#), which is operated by the California Institute of Technology, under contract with the National Aeronautics and Space Administration under the Exoplanet Exploration Program. T.H.F. and S.N thank Howard and Astrid Preston for their generous support. G.L. is grateful for the support from NASA 80NSSC20K0641 and 80NSSC20K0522. M.R. thanks the Heising-Simons Foundation for their support through Grant #2023-4478.

## APPENDIX

### A. THE IMPACT OF LYING NEAR A MEAN-MOTION RESONANCE

Of the six sweeping-resonant systems shown in Figure 6, two of them have planets that lie near mean-motion resonances (MMRs). The two outer planets of Kepler-9 are approximately 1% wide of a 2 : 1 commensurability, and the planets of Kepler-487 lie near a 32 : 5 : 2 commensurability. The outer planet’s orbit is much closer to the 16 : 1 commensurability with the inner planet than the 5 : 2 with the middle planet. Mean-motion resonances occur on orbital timescales, and are therefore not accounted for in the secular model used heretofore, requiring further investigation.

To verify that MMRs are not at play in these systems, we integrate Kepler-9 and Kepler-487 using different values of the outer planet semimajor axis and randomized inner planet initial inclination. This allows us to quantify how close these systems are to actually being in an MMR and to what extent that changes their behavior. We integrate using the N-body code REBOUND and use the add-on pack REBOUNDx with its implemented gravitational harmonics to incorporate a changing values of  $J_2$  using the WHFast integrator (Rein & Liu 2012; Tamayo et al. 2020; Rein & Tamayo 2015). The timestep for the WHFast integrator was set to be 3% of the shortest orbital period in the system. For Kepler-9 (Kepler-487), the outer planet’s semimajor axis was varied between a period ratio with the middle (inner) planet of 1.97 – 2.03 (1.59 – 16.1); the initial mutual inclination between outer planets was fixed to 2.5° (4.5°) for all integrations; the inner planet’s initial inclination was randomized uniformly between 0 – 3° (0 – 3°); and all other orbital elements were held constant between integrations. The integrations were run for  $5 \times 10^6$  years with a  $J_2$  evolution rate of 10 times what is shown in Figure 2. Faridani et al. (2023) found that such increased  $J_2$  evolution does not qualitatively affect the results and only minorly affects them quantitatively. Even at the increased evolution rate, the timescale of  $\dot{J}_2$  is still much slower than the Laplace-Lagrange timescales between the planets.

We show the results of these integrations in Figure 10, where we plot the period ratio between the outer two planets versus  $\Delta i_{mut}$  over the integrations. Both  $\Delta i_{mut,01}$  (red) and  $\Delta i_{mut,12}$  (blue) are shown. Both systems display no effect from the MMRs at their observed period ratios. For Kepler-9, wide of resonance (where the planets are observed to lie today) and short of the 2 : 1 resonance, the systems display similar behavior, producing similar mutual inclination

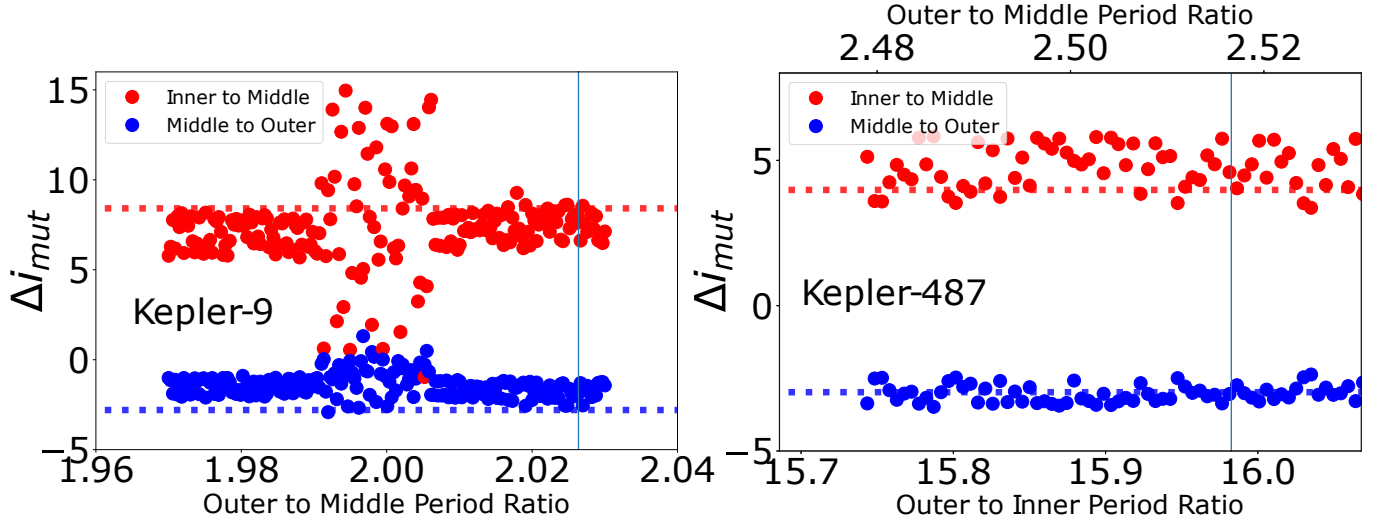


**Figure 10.** Relation between period ratio of outer two planets and  $\Delta i_{mut}$  for Kepler-9 (left) and relation between period ratio of outer two planets and outer/inner for Kepler-487. The changing of the period ratio was performed by changing the outer planet’s semimajor axis. The solid light blue lines represents the observed period ratios. The dotted red and blue lines represent the values of  $\Delta i_{mut}$  predicted by the fits for Kepler-9 and Kepler-487 shown in Figure 7.

excitation between the inner planet and the outer pair. However, on-resonance, the system exhibits chaotic behavior, where the inclinations and eccentricities of the planets vary within a broader range (consistent with observations; see e.g. Rice et al. (2023)). For Kepler-487, the outer and inner planets lie very close to a 16 : 1 ratio. However, the effect of the commensurability is negligible, with changes to the outer planet period not having an effect on the system’s evolution. This non-effect persists even when the 16 : 1 ratio is near-exact. Moreover, the outer two planets of Kepler-487 are too distant from the 5 : 2 commensurability for it to have an effect.

While neither Kepler-9 nor Kepler-487 lie close enough to their respective commensurabilities to impact the conclusions drawn from the secular calculations, this is not the case for all systems. As can be seen from the left panel of Figure 10, a 2 : 1 commensurability between outer planets can have significant effect on the change on  $\Delta i_{mut,01}$  caused by evolving  $J_2$ . For the integrations near the commensurability, the evolution became chaotic. However, that an orbit is chaotic does not mean that secular resonances via evolving  $J_2$  have no effect. Even in the chaotic regime, the mutual inclination between inner and middle planets almost always increases dramatically as  $J_2$  passes through the secular resonant value (though the chaos occasionally drives the inner and middle two planets to temporarily align again, reducing the value of  $\Delta i_{mut,01}$ ). Because these MMR configurations are chaotic, this may also drive the inner planet’s inclination even higher, potentially systematically removing such systems from transiting configurations, and therefore removing them from our sample.

## B. SWEEPING RESONANCE FROM $J_2$ , PLANETARY MIGRATION, AND THE DISK

The times we find these resonances occurring are relatively early in the system’s life ( $< 50$  Myr). During this same period or earlier, the protoplanetary disk is evaporating and the planets may be migrating. The protoplanetary disk introduces its own potential, and its evaporation may prompt resonances of its own (e.g., Heppenheimer 1980; Ward 1981; Nagasawa et al. 2003; Petrovich et al. 2020; Li & Lai 2023; Zanazzi & Chiang 2024). Planetary migration would cause a system’s location in  $a_1/a_0 - a_2/a_0$  space to vary, potentially interfering with the sweeping secular resonances from evolving  $J_2$ , and any mean-motion resonances the system passes through could have a significant impact as well.

Neither of these possibilities are taken into account in our model, which assumes that the system initial conditions may be sculpted by these processes, but that they are finished making significant impact by the time  $J_2$  begins evolving in our simulations at  $t = 10$  Myr. While protoplanetary disks typically evaporate in less than 10 Myr, older disks have been discovered, indicating the disk lifetime distribution may be wider than previously thought (see e.g. Silverberg et al. 2020; Pfalzner & Dincer 2024). Therefore, it is necessary to consider when  $J_2$  begins to evolve and whether that happens while the disk is still present.

The 10 Myr delay shown in Figure 2 is of somewhat arbitrary duration. However, the existence of a period where  $J_2$  is roughly constant before it starts decreasing due to stellar spin-down is not arbitrary. For example, Becker et al.

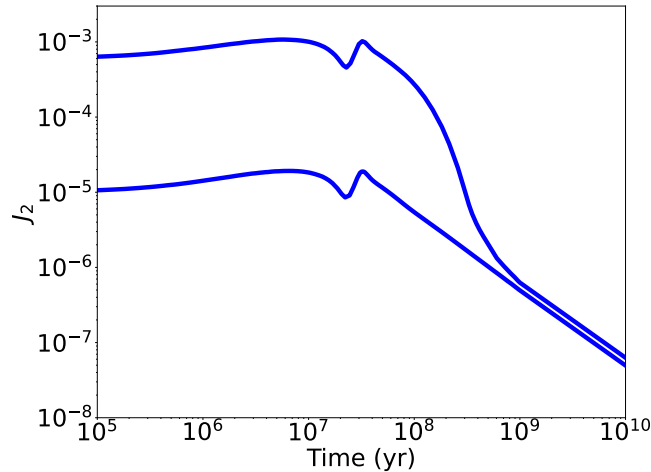


**Figure 11.** Model of  $J_2$  evolution for a  $1.1 M_\odot$  star. Stellar parameters were calculated by a MESA model (the same model as Figure 2), but spin evolution was calculated by the wind model given in Matt et al. (2015).

(2020) show in their Figure 5 the  $J_2$  evolution of a  $0.686 M_\odot$  star where  $J_2$  remains constant for the first 80 Myr of the star’s life. They calculate this using Baraffe et al. (2015)’s stellar models and Matt et al. (2015)’s wind model. Using that wind model but using a MESA model for a  $1.1 M_\odot$  star produces a  $\sim 60$  Myr lag before the  $J_2$  drops below its initial value (Paxton et al. 2011, 2013, 2015, 2018, 2019; Jermyn et al. 2023). This alternative  $J_2$  evolution is shown in Figure 11. After 60 Myr, the disk is almost certainly no longer causing significant precession and migration will have stopped. Therefore, we assume disk effects and migration need not be included in our simulations. If  $J_2$  begins to decrease early, then the initial  $J_2$  of the post-migration epoch will be lower than assumed here.

### C. THE SAMPLE OF 31 THREE-PLANET ALL-TRANSITING SYSTEMS

#### REFERENCES

- Albrecht, S. H., Marcussen, M. L., Winn, J. N., Dawson, R. I., & Knudstrup, E. 2021, *ApJL*, 916, L1, doi: [10.3847/2041-8213/ac0f03](https://doi.org/10.3847/2041-8213/ac0f03)
- Antoniadou, K. I., & Libert, A.-S. 2020, *A&A*, 640, A55, doi: [10.1051/0004-6361/202037779](https://doi.org/10.1051/0004-6361/202037779)
- Baraffe, I., Homeier, D., Allard, F., & Chabrier, G. 2015, *A&A*, 577, A42, doi: [10.1051/0004-6361/201425481](https://doi.org/10.1051/0004-6361/201425481)
- Barnes, S. A. 2003, *ApJ*, 586, 464, doi: [10.1086/367639](https://doi.org/10.1086/367639)
- Becker, J., Batygin, K., Fabrycky, D., et al. 2020, *AJ*, 160, 254, doi: [10.3847/1538-3881/abbad3](https://doi.org/10.3847/1538-3881/abbad3)
- Berger, T. A., Huber, D., Gaidos, E., & van Saders, J. L. 2018, *ApJ*, 866, 99, doi: [10.3847/1538-4357/aada83](https://doi.org/10.3847/1538-4357/aada83)
- Best, M., Sefilian, A. A., & Petrovich, C. 2024, *ApJ*, 960, 89, doi: [10.3847/1538-4357/ad0965](https://doi.org/10.3847/1538-4357/ad0965)
- Borsato, L., Marzari, F., Nascimbeni, V., et al. 2014, *A&A*, 571, A38, doi: [10.1051/0004-6361/201424080](https://doi.org/10.1051/0004-6361/201424080)
- Borsato, L., Malavolta, L., Piotto, G., et al. 2019, *MNRAS*, 484, 3233, doi: [10.1093/mnras/stz181](https://doi.org/10.1093/mnras/stz181)
- Brefka, L., & Becker, J. C. 2021, *AJ*, 162, 242, doi: [10.3847/1538-3881/ac2a32](https://doi.org/10.3847/1538-3881/ac2a32)
- Cabrera, J., Csizmadia, S., Lehmann, H., et al. 2014, *ApJ*, 781, 18, doi: [10.1088/0004-637X/781/1/18](https://doi.org/10.1088/0004-637X/781/1/18)
- Chen, C., Li, G., & Petrovich, C. 2022, *ApJ*, 930, 58, doi: [10.3847/1538-4357/ac6024](https://doi.org/10.3847/1538-4357/ac6024)
- Cochran, W. D., Fabrycky, D. C., Torres, G., et al. 2011, *ApJS*, 197, 7, doi: [10.1088/0067-0049/197/1/7](https://doi.org/10.1088/0067-0049/197/1/7)
- Crossfield, I. J. M., Ciardi, D. R., Petigura, E. A., et al. 2016, *ApJS*, 226, 7, doi: [10.3847/0067-0049/226/1/7](https://doi.org/10.3847/0067-0049/226/1/7)
- de Leon, J. P., Livingston, J., Endl, M., et al. 2021, *MNRAS*, 508, 195, doi: [10.1093/mnras/stab2305](https://doi.org/10.1093/mnras/stab2305)
- Delorme, P., Cameron, A. C., Hebb, L., et al. 2011, in *Astronomical Society of the Pacific Conference Series*, Vol. 448, 16th Cambridge Workshop on Cool Stars, Stellar Systems, and the Sun, ed. C. Johns-Krull, M. K. Browning, & A. A. West, 841

Name	$M_*$ ( $M_\odot$ )	$R_*$ ( $R_\odot$ )	Star Reference	$a_0$ (au)	$a_1$ (au)	$a_2$ (au)	$m_0$ ( $M_\oplus$ )	$m_1$ ( $M_\oplus$ )	$m_2$ ( $M_\oplus$ )	Planet Reference(s)
Kepler-9	1.07	1.02	Torres et al. (2011)	0.027 <sup>†</sup>	0.143*	0.230*	3.342 <sup>†</sup>	<b>43.4*</b>	<b>29.9*</b>	<sup>†</sup> Torres et al. (2011); *Borsato et al. (2019)
Kepler-619	1.09	1.11	Mo16	0.022 <sup>†</sup>	0.062 <sup>†</sup>	0.103*	3.596 <sup>†</sup>	14.72 <sup>†</sup>	22.56*	<sup>†</sup> Mo16; *Stassun et al. (2019)
Kepler-487	0.91	0.88	Mo16	0.033 <sup>†</sup>	0.115*	0.213*	12.06 <sup>†</sup>	106.3*	11.43*	<sup>†</sup> V22; *Mo16
K2-198	0.8	0.76	Hedges et al. (2019)	0.040	0.069	0.120	2.364	9.882	22.72	Hedges et al. (2019)
Kepler-529	1.07	1.14	Mo16	0.031 <sup>†</sup>	0.109 <sup>†</sup>	0.217*	4.543 <sup>†</sup>	5.422 <sup>†</sup>	12.19*	<sup>†</sup> Mo16; *V22
EPIC 249893012	1.05	1.70 <sup>+</sup>	Hidalgo et al. (2020)	0.046	0.124	0.215	<b>8.75</b>	<b>14.67</b>	<b>10.18</b>	Hidalgo et al. (2020)
HD 22946	1.1	1.12	Garai et al. (2023)	0.051	0.091	0.264	2.124	9.205	10.95	Garai et al. (2023)
HD 28109	1.26	1.45	Dransfield et al. (2022)	0.170	0.309	0.406	18.49	7.943	5.681	Dransfield et al. (2022)
K2-19	0.88	0.82	Petigura (2020)	0.034	0.074	0.097	1.289	32.4	10.8	Petigura (2020)
K2-219	1.02	1.19	Ma18	0.048	0.069	0.098	2.071	2.425	10.75	Ma18
K2-352	0.98	0.95	de Leon et al. (2021)	0.046	0.079	0.117	2.155	4.908	8.615	de Leon et al. (2021)
K2-37	0.9	0.85	Simukoff et al. (2016)	0.051	0.065	0.110	3.194	11.89	11.76	Simukoff et al. (2016)
K2-58	0.89	0.85	Crossfield et al. (2016)	0.035	0.069	0.151	3.243	11.43	3.700	Crossfield et al. (2016)
K2-80	0.9	0.86	Crossfield et al. (2016)	0.059 <sup>†</sup>	0.134 <sup>†</sup>	0.177*	2.559 <sup>†</sup>	5.489 <sup>†</sup>	10.60*	<sup>†</sup> Crossfield et al. (2016); * Ma18
Kepler-1073	0.92	1.12	Thompson et al. (2018a)	0.035	0.048	0.080	2.636	3.342	9.035	Thompson et al. (2018a)
Kepler-1530	0.92	0.88	Mo16	0.035 <sup>†</sup>	0.058 <sup>†</sup>	0.083*	3.342 <sup>†</sup>	3.391 <sup>†</sup>	15.59*	<sup>†</sup> Mo16; *V22
Kepler-18	0.97	1.11	Cochran et al. (2011)	0.044	0.075	0.117	<b>6.9</b>	<b>17.3</b>	<b>16.4</b>	Cochran et al. (2011)
Kepler-27	0.95	0.85	Mo16	0.066 <sup>†</sup>	0.117*	0.189*	11.60 <sup>†</sup>	21.16*	28.92*	<sup>†</sup> V22; *Steffen et al. (2012)
Kepler-271	0.9	0.87	Mo16	0.057 <sup>†</sup>	0.071*	0.090*	0.362 <sup>†</sup>	0.882*	1.656*	<sup>†</sup> Mo16; *Rowe et al. (2014)
Kepler-289	1.08	1.0	Schmitt et al. (2014)	0.212	0.328	0.504	<b>7.3</b>	<b>4.0</b>	<b>132.0</b>	Schmitt et al. (2014)
Kepler-30	0.99	0.95	Sanchis-Ojeda et al. (2012)	0.185	0.300	0.534	11.3	640.0	23.09	Sanchis-Ojeda et al. (2012)
Kepler-31	1.21	1.22	Fabrycky et al. (2012)	0.158	0.254	0.411	34.55	32.63	20.35	Fabrycky et al. (2012)
Kepler-431	1.07	1.09	Everett et al. (2015)	0.071	0.084	0.104	0.518	0.373	1.289	Everett et al. (2015)
Kepler-450	1.19	1.64	Stassun et al. (2019)	0.079	0.128	0.193	0.647	11.04	40.92	Van Eylen & Albrecht (2015)
Kepler-51	1.04	0.93	Masuda (2014)	0.251	0.384	0.509	<b>2.1</b>	<b>4.0</b>	<b>7.6</b>	Masuda (2014)
Kepler-549	0.9	0.85	Thompson et al. (2018b)	0.157	0.228	0.445	22.81	10.71	13.11	Thompson et al. (2018b)
Kepler-616	0.98	0.97	Mo16	0.090 <sup>†</sup>	0.267*	0.391 <sup>†</sup>	9.832 <sup>†</sup>	11.25 <sup>†</sup>	16.56*	<sup>†</sup> Mo16; *V22
Kepler-770	0.94	0.92	Mo16	0.024	0.049	0.136	1.560	2.272	9.035	Mo16
KOI-7892	1.15	1.24	Stassun et al. (2019)	0.099 <sup>†</sup>	0.205*	0.365*	13.49 <sup>†</sup>	21.98*	9.646*	<sup>†</sup> V22; *Wang et al. (2015)
KOI-125	0.86	0.85	Nielsen et al. (2020)	0.051	0.081	0.137	<b>9.5</b>	<b>6.629</b>	<b>13.6</b>	Nielsen et al. (2020)
TOI-2076	0.82	0.77	Osborn et al. (2022)	0.087	0.139	0.196	10.38	17.21	15.24	Osborn et al. (2022)

**Table 5.** Parameters adopted for the 31-system sample. All semimajor axes were derived from orbital periods rather than reported semimajor axes in listed references, to ensure that period ratios are maintained. Bolded masses were adopted from references, and unbolded masses were derived from the mass-radius relation derived in Miller et al. (2023). †: See discussion of EPIC 249893012’s radius in Section 4.1. Morton et al. (2016), Valizadegan et al. (2022), and Mayo et al. (2018) are abbreviated as Mo16, Va22, and Ma18 respectively.

- Denham, P., Naoz, S., Hoang, B.-M., Stephan, A. P., & Farr, W. M. 2019, *MNRAS*, 482, 4146, doi: [10.1093/mnras/sty2830](https://doi.org/10.1093/mnras/sty2830)
- Dobbs-Dixon, I., Lin, D. N. C., & Mardling, R. A. 2004, *ApJ*, 610, 464, doi: [10.1086/421510](https://doi.org/10.1086/421510)
- Dransfield, G., Triaud, A. H. M. J., Guillot, T., et al. 2022, *MNRAS*, 515, 1328, doi: [10.1093/mnras/stac1383](https://doi.org/10.1093/mnras/stac1383)
- Everett, M. E., Barclay, T., Ciardi, D. R., et al. 2015, *AJ*, 149, 55, doi: [10.1088/0004-6256/149/2/55](https://doi.org/10.1088/0004-6256/149/2/55)
- Fabrycky, D. C., Ford, E. B., Steffen, J. H., et al. 2012, *ApJ*, 750, 114, doi: [10.1088/0004-637X/750/2/114](https://doi.org/10.1088/0004-637X/750/2/114)
- Fabrycky, D. C., Lissauer, J. J., Ragozzine, D., et al. 2014, *ApJ*, 790, 146, doi: [10.1088/0004-637X/790/2/146](https://doi.org/10.1088/0004-637X/790/2/146)
- Fang, J., & Margot, J.-L. 2012, *ApJ*, 761, 92, doi: [10.1088/0004-637X/761/2/92](https://doi.org/10.1088/0004-637X/761/2/92)
- Faridani, T. H., Naoz, S., Li, G., & Inzunza, N. 2023, *ApJ*, 956, 90, doi: [10.3847/1538-4357/acf378](https://doi.org/10.3847/1538-4357/acf378)
- Faridani, T. H., Naoz, S., Wei, L., & Farr, W. M. 2022, *ApJ*, 932, 78, doi: [10.3847/1538-4357/ac6e38](https://doi.org/10.3847/1538-4357/ac6e38)
- Freudenthal, J., von Essen, C., Dreizler, S., et al. 2018, *A&A*, 618, A41, doi: [10.1051/0004-6361/201833436](https://doi.org/10.1051/0004-6361/201833436)
- Gallet, F., & Bouvier, J. 2013, *A&A*, 556, A36, doi: [10.1051/0004-6361/201321302](https://doi.org/10.1051/0004-6361/201321302)
- Garai, Z., Osborn, H. P., Gandolfi, D., et al. 2023, *A&A*, 674, A44, doi: [10.1051/0004-6361/202345943](https://doi.org/10.1051/0004-6361/202345943)
- Gillon, M., Jehin, E., Lederer, S. M., et al. 2016, *Nature*, 533, 221, doi: [10.1038/nature17448](https://doi.org/10.1038/nature17448)
- Gupta, A., & Schlichting, H. E. 2021, *MNRAS*, 504, 4634, doi: [10.1093/mnras/stab1128](https://doi.org/10.1093/mnras/stab1128)
- Hadden, S., & Lithwick, Y. 2014, *ApJ*, 787, 80, doi: [10.1088/0004-637X/787/1/80](https://doi.org/10.1088/0004-637X/787/1/80)
- . 2017, *AJ*, 154, 5, doi: [10.3847/1538-3881/aa71ef](https://doi.org/10.3847/1538-3881/aa71ef)
- Hansen, B. M. S., & Murray, N. 2015, *MNRAS*, 448, 1044, doi: [10.1093/mnras/stv049](https://doi.org/10.1093/mnras/stv049)
- Hansen, B. M. S., & Naoz, S. 2020, *MNRAS*, 499, 1682, doi: [10.1093/mnras/staa2602](https://doi.org/10.1093/mnras/staa2602)
- Hartman, J. D., Bakos, G. Á., Kovács, G., & Noyes, R. W. 2010, *MNRAS*, 408, 475, doi: [10.1111/j.1365-2966.2010.17147.x](https://doi.org/10.1111/j.1365-2966.2010.17147.x)
- Hedges, C., Saunders, N., Barentsen, G., et al. 2019, *ApJL*, 880, L5, doi: [10.3847/2041-8213/ab2a74](https://doi.org/10.3847/2041-8213/ab2a74)
- Hedges, C., Hughes, A., Zhou, G., et al. 2021, *AJ*, 162, 54, doi: [10.3847/1538-3881/ac06cd](https://doi.org/10.3847/1538-3881/ac06cd)
- Heppenheimer, T. A. 1980, *Icarus*, 41, 76, doi: [10.1016/0019-1035\(80\)90160-8](https://doi.org/10.1016/0019-1035(80)90160-8)
- Hidalgo, D., Pallé, E., Alonso, R., et al. 2020, *A&A*, 636, A89, doi: [10.1051/0004-6361/201937080](https://doi.org/10.1051/0004-6361/201937080)
- Holczer, T., Mazeh, T., Nachmani, G., et al. 2016, *ApJS*, 225, 9, doi: [10.3847/0067-0049/225/1/9](https://doi.org/10.3847/0067-0049/225/1/9)
- Holman, M. J., Fabrycky, D. C., Ragozzine, D., et al. 2010, *Science*, 330, 51, doi: [10.1126/science.1195778](https://doi.org/10.1126/science.1195778)
- Jermyn, A. S., Bauer, E. B., Schwab, J., et al. 2023, *ApJS*, 265, 15, doi: [10.3847/1538-4365/aca8d](https://doi.org/10.3847/1538-4365/aca8d)
- Kraft, R. P. 1967, *ApJ*, 150, 551, doi: [10.1086/149359](https://doi.org/10.1086/149359)
- Lanza, A. F., & Shkolnik, E. L. 2014, *MNRAS*, 443, 1451, doi: [10.1093/mnras/stu1206](https://doi.org/10.1093/mnras/stu1206)
- Li, J., & Lai, D. 2023, *ApJ*, 956, 17, doi: [10.3847/1538-4357/aced89](https://doi.org/10.3847/1538-4357/aced89)
- Lissauer, J. J., Ragozzine, D., Fabrycky, D. C., et al. 2011, *ApJS*, 197, 8, doi: [10.1088/0067-0049/197/1/8](https://doi.org/10.1088/0067-0049/197/1/8)
- Lithwick, Y., & Wu, Y. 2011, *ApJ*, 739, 31, doi: [10.1088/0004-637X/739/1/31](https://doi.org/10.1088/0004-637X/739/1/31)
- Lu, T., An, Q., Li, G., et al. 2024, arXiv e-prints, arXiv:2405.19511, doi: [10.48550/arXiv.2405.19511](https://doi.org/10.48550/arXiv.2405.19511)
- Marzari, F., & Nagasawa, M. 2020, *MNRAS*, 493, 427, doi: [10.1093/mnras/staa271](https://doi.org/10.1093/mnras/staa271)
- Masuda, K. 2014, *ApJ*, 783, 53, doi: [10.1088/0004-637X/783/1/53](https://doi.org/10.1088/0004-637X/783/1/53)
- Matt, S. P., Brun, A. S., Baraffe, I., Bouvier, J., & Chabrier, G. 2015, *ApJL*, 799, L23, doi: [10.1088/2041-8205/799/2/L23](https://doi.org/10.1088/2041-8205/799/2/L23)
- Mayo, A. W., Vanderburg, A., Latham, D. W., et al. 2018, *AJ*, 155, 136, doi: [10.3847/1538-3881/aaadff](https://doi.org/10.3847/1538-3881/aaadff)
- Meibom, S., Barnes, S. A., Platais, I., et al. 2015, *Nature*, 517, 589, doi: [10.1038/nature14118](https://doi.org/10.1038/nature14118)
- Mestel, L. 1968, *MNRAS*, 138, 359, doi: [10.1093/mnras/138.3.359](https://doi.org/10.1093/mnras/138.3.359)
- Millholland, S., & Spalding, C. 2020, arXiv e-prints, arXiv:2010.15087. <https://arxiv.org/abs/2010.15087>
- Millholland, S., Wang, S., & Laughlin, G. 2017, *ApJL*, 849, L33, doi: [10.3847/2041-8213/aa9714](https://doi.org/10.3847/2041-8213/aa9714)
- Morton, T. D., Bryson, S. T., Coughlin, J. L., et al. 2016, *ApJ*, 822, 86, doi: [10.3847/0004-637X/822/2/86](https://doi.org/10.3847/0004-637X/822/2/86)
- Müller, S., Baron, J., Helled, R., Bouchy, F., & Parc, L. 2023, arXiv e-prints, arXiv:2311.12593, doi: [10.48550/arXiv.2311.12593](https://doi.org/10.48550/arXiv.2311.12593)
- Murchikova, L., & Tremaine, S. 2020, *AJ*, 160, 160, doi: [10.3847/1538-3881/abab9e](https://doi.org/10.3847/1538-3881/abab9e)
- Murray, C. D., & Dermott, S. F. 2000, *Solar System Dynamics*
- Nagasawa, M., Lin, D. N. C., & Ida, S. 2003, *ApJ*, 586, 1374, doi: [10.1086/367884](https://doi.org/10.1086/367884)
- Naoz, S., Farr, W. M., Lithwick, Y., Rasio, F. A., & Teyssandier, J. 2013a, *MNRAS*, 431, 2155, doi: [10.1093/mnras/stt302](https://doi.org/10.1093/mnras/stt302)
- Naoz, S., Kocsis, B., Loeb, A., & Yunes, N. 2013b, *ApJ*, 773, 187, doi: [10.1088/0004-637X/773/2/187](https://doi.org/10.1088/0004-637X/773/2/187)
- NASA Exoplanet Science Institute. 2024, Planetary Systems Table, IPAC, doi: [10.26133/NEA12](https://doi.org/10.26133/NEA12)

- Nielsen, L. D., Gandolfi, D., Armstrong, D. J., et al. 2020, *MNRAS*, 492, 5399, doi: [10.1093/mnras/staa197](https://doi.org/10.1093/mnras/staa197)
- O'Connor, C. E., Teyssandier, J., & Lai, D. 2022, *MNRAS*, 513, 4178, doi: [10.1093/mnras/stac1189](https://doi.org/10.1093/mnras/stac1189)
- Osborn, H. P., Bonfanti, A., Gandolfi, D., et al. 2022, *A&A*, 664, A156, doi: [10.1051/0004-6361/202243065](https://doi.org/10.1051/0004-6361/202243065)
- Parker, E. N. 1958, *Physics of Fluids*, 1, 171, doi: [10.1063/1.1724339](https://doi.org/10.1063/1.1724339)
- Paxton, B., Bildsten, L., Dotter, A., et al. 2011, *ApJS*, 192, 3, doi: [10.1088/0067-0049/192/1/3](https://doi.org/10.1088/0067-0049/192/1/3)
- Paxton, B., Cantiello, M., Arras, P., et al. 2013, *ApJS*, 208, 4, doi: [10.1088/0067-0049/208/1/4](https://doi.org/10.1088/0067-0049/208/1/4)
- Paxton, B., Marchant, P., Schwab, J., et al. 2015, *ApJS*, 220, 15, doi: [10.1088/0067-0049/220/1/15](https://doi.org/10.1088/0067-0049/220/1/15)
- Paxton, B., Schwab, J., Bauer, E. B., et al. 2018, *ApJS*, 234, 34, doi: [10.3847/1538-4365/aaa5a8](https://doi.org/10.3847/1538-4365/aaa5a8)
- Paxton, B., Smolec, R., Schwab, J., et al. 2019, *ApJS*, 243, 10, doi: [10.3847/1538-4365/ab2241](https://doi.org/10.3847/1538-4365/ab2241)
- Petigura, E. A. 2020, *AJ*, 160, 89, doi: [10.3847/1538-3881/ab9fff](https://doi.org/10.3847/1538-3881/ab9fff)
- Petrovich, C., Deibert, E., & Wu, Y. 2019, *AJ*, 157, 180, doi: [10.3847/1538-3881/ab0e0a](https://doi.org/10.3847/1538-3881/ab0e0a)
- Petrovich, C., Muñoz, D. J., Kratter, K. M., & Malhotra, R. 2020, *ApJL*, 902, L5, doi: [10.3847/2041-8213/abb952](https://doi.org/10.3847/2041-8213/abb952)
- Pfalzner, S., & Dincer, F. 2024, *ApJ*, 963, 122, doi: [10.3847/1538-4357/ad1bef](https://doi.org/10.3847/1538-4357/ad1bef)
- Plavchan, P., Chen, X., & Pohl, G. 2015, *ApJ*, 805, 174, doi: [10.1088/0004-637X/805/2/174](https://doi.org/10.1088/0004-637X/805/2/174)
- Pu, B., & Lai, D. 2019, *MNRAS*, 488, 3568, doi: [10.1093/mnras/stz1817](https://doi.org/10.1093/mnras/stz1817)
- Pu, B., & Wu, Y. 2015, *ApJ*, 807, 44, doi: [10.1088/0004-637X/807/1/44](https://doi.org/10.1088/0004-637X/807/1/44)
- Rein, H., & Liu, S. F. 2012, *A&A*, 537, A128, doi: [10.1051/0004-6361/201118085](https://doi.org/10.1051/0004-6361/201118085)
- Rein, H., & Tamayo, D. 2015, *MNRAS*, 452, 376, doi: [10.1093/mnras/stv1257](https://doi.org/10.1093/mnras/stv1257)
- Rice, M., Wang, X.-Y., Wang, S., et al. 2023, *AJ*, 166, 266, doi: [10.3847/1538-3881/ad09de](https://doi.org/10.3847/1538-3881/ad09de)
- Rowe, J. F., Bryson, S. T., Marcy, G. W., et al. 2014, *The Astrophysical Journal*, 784, 45, doi: [10.1088/0004-637x/784/1/45](https://doi.org/10.1088/0004-637x/784/1/45)
- Sanchis-Ojeda, R., Fabrycky, D. C., Winn, J. N., et al. 2012, *Nature*, 487, 449, doi: [10.1038/nature11301](https://doi.org/10.1038/nature11301)
- Schatzman, E. 1962, *Annales d'Astrophysique*, 25, 18
- Schmitt, J. R., Agol, E., Deck, K. M., et al. 2014, *ApJ*, 795, 167, doi: [10.1088/0004-637X/795/2/167](https://doi.org/10.1088/0004-637X/795/2/167)
- Shallue, C. J., & Vanderburg, A. 2018, *AJ*, 155, 94, doi: [10.3847/1538-3881/aa9e09](https://doi.org/10.3847/1538-3881/aa9e09)
- Silverberg, S. M., Wisniewski, J. P., Kuchner, M. J., et al. 2020, *ApJ*, 890, 106, doi: [10.3847/1538-4357/ab68e6](https://doi.org/10.3847/1538-4357/ab68e6)
- Sinukoff, E., Howard, A. W., Petigura, E. A., et al. 2016, *ApJ*, 827, 78, doi: [10.3847/0004-637X/827/1/78](https://doi.org/10.3847/0004-637X/827/1/78)
- Skumanich, A. 1972, *ApJ*, 171, 565, doi: [10.1086/151310](https://doi.org/10.1086/151310)
- Spalding, C., & Batygin, K. 2016, *ApJ*, 830, 5, doi: [10.3847/0004-637X/830/1/5](https://doi.org/10.3847/0004-637X/830/1/5)
- Spalding, C., Marx, N. W., & Batygin, K. 2018, *AJ*, 155, 167, doi: [10.3847/1538-3881/aab43a](https://doi.org/10.3847/1538-3881/aab43a)
- Stassun, K. G., Oelkers, R. J., Paegert, M., et al. 2019, *AJ*, 158, 138, doi: [10.3847/1538-3881/ab3467](https://doi.org/10.3847/1538-3881/ab3467)
- Steffen, J. H., Fabrycky, D. C., Ford, E. B., et al. 2012, *MNRAS*, 421, 2342, doi: [10.1111/j.1365-2966.2012.20467.x](https://doi.org/10.1111/j.1365-2966.2012.20467.x)
- Stephan, A. P., & Gaudi, B. S. 2023, *ApJ*, 950, 32, doi: [10.3847/1538-4357/accd6b](https://doi.org/10.3847/1538-4357/accd6b)
- Tamayo, D., Rein, H., Shi, P., & Hernandez, D. M. 2020, *MNRAS*, 491, 2885, doi: [10.1093/mnras/stz2870](https://doi.org/10.1093/mnras/stz2870)
- Thompson, S. E., Coughlin, J. L., Hoffman, K., et al. 2018a, *ApJS*, 235, 38, doi: [10.3847/1538-4365/aab4f9](https://doi.org/10.3847/1538-4365/aab4f9)
- . 2018b, *ApJS*, 235, 38, doi: [10.3847/1538-4365/aab4f9](https://doi.org/10.3847/1538-4365/aab4f9)
- Torres, G., Fressin, F., Batalha, N. M., et al. 2011, *ApJ*, 727, 24, doi: [10.1088/0004-637X/727/1/24](https://doi.org/10.1088/0004-637X/727/1/24)
- Valizadegan, H., Martinho, M. J. S., Wilkens, L. S., et al. 2022, *ApJ*, 926, 120, doi: [10.3847/1538-4357/ac4399](https://doi.org/10.3847/1538-4357/ac4399)
- Van Eylen, V., & Albrecht, S. 2015, *ApJ*, 808, 126, doi: [10.1088/0004-637X/808/2/126](https://doi.org/10.1088/0004-637X/808/2/126)
- Van Eylen, V., Albrecht, S., Huang, X., et al. 2019, *AJ*, 157, 61, doi: [10.3847/1538-3881/aaf22f](https://doi.org/10.3847/1538-3881/aaf22f)
- Van Laerhoven, C., & Greenberg, R. 2012, *Celestial Mechanics and Dynamical Astronomy*, 113, 215, doi: [10.1007/s10569-012-9410-6](https://doi.org/10.1007/s10569-012-9410-6)
- Volk, K., & Malhotra, R. 2020, *AJ*, 160, 98, doi: [10.3847/1538-3881/aba0b0](https://doi.org/10.3847/1538-3881/aba0b0)
- Wang, J., Fischer, D. A., Barclay, T., et al. 2015, *ApJ*, 815, 127, doi: [10.1088/0004-637X/815/2/127](https://doi.org/10.1088/0004-637X/815/2/127)
- Wang, S., Jones, M., Shporer, A., et al. 2018, *ArXiv e-prints*. <https://arxiv.org/abs/1810.02341>
- Ward, W. R. 1981, *Icarus*, 47, 234, doi: [10.1016/0019-1035\(81\)90169-X](https://doi.org/10.1016/0019-1035(81)90169-X)
- Ward, W. R., Colombo, G., & Franklin, F. A. 1976, *Icarus*, 28, 441, doi: [10.1016/0019-1035\(76\)90117-2](https://doi.org/10.1016/0019-1035(76)90117-2)
- Weber, E. J., & Davis, Leverett, J. 1967, *ApJ*, 148, 217, doi: [10.1086/149138](https://doi.org/10.1086/149138)
- Wei, L., Naoz, S., Faridani, T., & Farr, W. M. 2021, *ApJ*, 923, 118, doi: [10.3847/1538-4357/ac2c70](https://doi.org/10.3847/1538-4357/ac2c70)
- Weiss, L. M., Millholland, S. C., Petigura, E. A., et al. 2023, in *Astronomical Society of the Pacific Conference Series*, Vol. 534, *Protostars and Planets VII*, ed. S. Inutsuka, Y. Aikawa, T. Muto, K. Tomida, & M. Tamura, 863
- Weiss, L. M., & Petigura, E. A. 2020, *The Astrophysical Journal*, 893, L1, doi: [10.3847/2041-8213/ab7c69](https://doi.org/10.3847/2041-8213/ab7c69)

Weiss, L. M., Marcy, G. W., Petigura, E. A., et al. 2018,  
AJ, 155, 48, doi: [10.3847/1538-3881/aa9ff6](https://doi.org/10.3847/1538-3881/aa9ff6)

Weiss, L. M., Isaacson, H., Howard, A. W., et al. 2024,  
ApJS, 270, 8, doi: [10.3847/1538-4365/ad0cab](https://doi.org/10.3847/1538-4365/ad0cab)

Zanazzi, J. J., & Chiang, E. 2024, MNRAS, 527, 7203,  
doi: [10.1093/mnras/stad3066](https://doi.org/10.1093/mnras/stad3066)

Zhu, W. 2020, AJ, 159, 188, doi: [10.3847/1538-3881/ab7814](https://doi.org/10.3847/1538-3881/ab7814)

Zhu, W., Petrovich, C., Wu, Y., Dong, S., & Xie, J. 2018,  
ApJ, 860, 101, doi: [10.3847/1538-4357/aac6d5](https://doi.org/10.3847/1538-4357/aac6d5)